

Review

# Recent Developments for the Application of 3D Structured Material Nickel Foam and Graphene Foam in Direct Liquid Fuel Cells and Electrolyzers

Nabila A. Karim <sup>1,\*</sup> , Muhammad Syafiq Alias <sup>1</sup> and Hsiharng Yang <sup>2,3,\*</sup> 

<sup>1</sup> Fuel Cell Institute, Universiti Kebangsaan Malaysia, Bangi 43600, Selangor, Malaysia; muhammadsyafiq569@gmail.com

<sup>2</sup> Graduate Institute of Precision Engineering, National Chung Hsing University, 145 Xingda Road, South District, Taichung City 402, Taiwan

<sup>3</sup> Innovation and Development Center of Sustainable Agriculture (IDCSA), National Chung Hsing University, 145 Xingda Road, South District, Taichung City 402, Taiwan

\* Correspondence: nabila.akarim@ukm.edu.my (N.A.K.); hsiharng@dragon.nchu.edu.tw (H.Y.)

**Abstract:** Platinum and platinum-based catalysts are some of the most effective catalysts used in fuel cells. However, electrocatalysts used for direct liquid fuel cells (DLFCs) and electrolyzers are high cost and suffer from several other problems, thus hindering their commercialization as power sources to produce clean energy. Common issues in electrocatalysts are low stability and durability, slow kinetics, catalyst poisoning, high catalyst loading, high cost of the catalytic materials, poisoning of the electrocatalysts, and formation of intermediate products during electrochemical reactions. The use of catalyst supports can enhance the catalytic activity and stability of the power sources. Thus, nickel foam and graphene foam with 3D structures have advantages over other catalyst supports. This paper presents the application of nickel foam and graphene foam as catalyst supports that enhance the activities, selectivity, efficiency, specific surface area, and exposure of the active sites of DLFCs. Selected recent studies on the use of foam in electrolyzers are also presented.

**Keywords:** nickel foam; graphene foam; support; electrocatalyst; porous



**Citation:** Karim, N.A.; Alias, M.S.; Yang, H. Recent Developments for the Application of 3D Structured Material Nickel Foam and Graphene Foam in Direct Liquid Fuel Cells and Electrolyzers. *Catalysts* **2021**, *11*, 279. <https://doi.org/10.3390/catal11020279>

Academic Editor: Vincenzo Baglio

Received: 12 January 2021

Accepted: 15 February 2021

Published: 19 February 2021

**Publisher's Note:** MDPI stays neutral with regard to jurisdictional claims in published maps and institutional affiliations.



**Copyright:** © 2021 by the authors. Licensee MDPI, Basel, Switzerland. This article is an open access article distributed under the terms and conditions of the Creative Commons Attribution (CC BY) license (<https://creativecommons.org/licenses/by/4.0/>).

## 1. Introduction

An economical, efficient and clean alternative energy is needed to replace the increasingly used fossil fuel due to increasing energy demands, which has caused the reservoir of fossil fuels to be depleted and high CO<sub>2</sub> emissions [1–3]. These problems have led to the use of fuel cells, an alternative which can generate electricity from chemical energy without combustion [4]. Direct liquid fuel cells (DLFCs) have many advantages, such as high energy density and efficiency, fast start-up, easy refueling, storage, and transport, low operating temperature, and environmental friendliness [5–7], compared to other types of fuel cells, especially the polymer electrolyte membrane fuel cells (PEMFCs) that use hydrogen as fuel.

The liquid fuels that are usually used in DLFCs are methanol, ethanol, formic acid, ethylene glycol, glycerol, urea, ammonia, hydrogen peroxide, and many others [8–11]. Each liquid fuel in DLFCs has different electrochemical reactions, energy densities, and theoretical cell potentials [8]. For example, crossover occurs a lot in Direct Methanol Fuel Cells because the methanol molecule is smaller than other type of liquid fuel such as ethanol and glycerol. The fuel crossover occurs when fuel is transported from anode to cathode through membrane and will reduce use of the fuel. However, in the fuel oxidation reaction, methanol is easier to convert to other products than ethanol and glycerol. The C–C bonds in ethanol and glycerol require higher activation energy to form another product [12,13].

The electrolyzers are used to produce a high purity of hydrogen on a large scale. Water splitting in an alkaline medium suffers from sluggish reaction because it requires an

additional water dissociation step [14]. To reduce the cost of platinum material, studies have focused on the use of non-noble metal, binary, and ternary alloy metals, but catalytic activity is not as high as platinum [14]. High pores are needed to increase the reaction activity because they can expose the active site to the reactant and accelerate the mass transfer. High pores also provide a high specific surface area to increase the reaction rate [15]. The use of foam as support increases the reaction activity in the electrolyzer.

Meanwhile, the energy output and efficiency of DLFCs are still low due to several challenges that need to be overcome. The technical challenges in DLFCs are liquid fuel crossover, poor mass transport, sluggish reaction rates, cathode flooding, chemical safety, species and thermal management, the production of side products, and the high-cost of catalysts [8,10,16,17]. The mass transport that occurs during the electrochemical reaction is poor due to the removal of reaction products from the catalyst surface and charge transfer in the cell [16]. The sluggish reaction rate and other problems related to the electrochemical reactions in DLFCs are the main challenges to overcome so that the commercialization of fuel cells can be sped up, especially to produce the catalysts for large-scale applications [18,19].

## 2. Challenges in Conventional Catalyst Support and Future Perspective Using 3D Structured Material Foam in DLFC

Membrane Electrolyte Assembly (MEA) serves as the heart of DLFCs since the electrochemical reaction that produces electricity occurs in this component. In addition to the problems with the electrochemical reaction occurring in DLFCs, other problems that have not been solved are the low stability and durability, slow kinetics, catalyst poisoning, high catalyst loading, high cost of the catalytic materials, poisoning of the electrocatalysts, and formation of the intermediate products during the electrochemical reactions [5,7,20]. The catalyst developed for the electrochemical reaction in DLFCs must meet the requirements, including a large surface area, low surface poisoning, a high porosity, multiple active sites for the reaction to occur, high activity, good conductivity, and long-term stability [20,21]. One of the strategies used to meet these criteria is use of catalyst support. Catalyst support is important to help distribute the nanoparticle catalyst and solve sluggish reaction problems in DLFCs [22]. Among the most commonly used catalyst supports are carbon black, carbon aerogels, carbon nanotubes, mesoporous carbon, graphene oxide, and graphene nanosheets [6,23,24], but these materials face problems, namely, their corrosion resistance [25,26] leads to particle detachment, Ostwald ripening, and agglomeration [27,28]. Therefore, the development of catalyst supports assists the catalyst in enhancing the catalytic activities, selectivity, efficiency, specific surface area, exposure of the active sites [20], durability, mechanical stability, and porosity, as well as conductivity [29,30] in the harsh environment.

During long runs, the catalyst on the electrode material is easily detached from the electrode surface, thus reducing the activity performance [31]. Therefore, stable catalyst support with highly exposed active facets, a high surface area, a strong corrosion resistance, chemical stability, high mechanical stability, excellent conductivity, and a special structure is required to support nanoparticle-sized catalysts [23,32,33]. Support material that has a large surface-to-volume ratio and strong binding of the nanoparticle catalyst on the support can enhance the catalytic activity of the electrochemical reaction in fuel cells [29,34,35]. The advantages of having a high surface area can also reduce the loading of the nanoparticles while smoothly increasing the number of active sites for the catalytic reaction to occur due to the highly distributed catalyst [30].

Nickel metal catalysts have a low reactivity towards the electrochemical reaction that occurs in fuel cells [36,37]; however, the nickel foam (NF) and graphene foam (GF) shown in Figure 1 [38] and Figure 2 [39], which have a 3D network structure, have high conductivity, controllable electrochemical properties, an excellent mechanical strength [37,40], a high surface area, a high porosity, and a low cost, and are suitable for use as catalyst supports [6,24,41,42]. A 3D network structure or skeleton structure provides a large surface area in NF and helps reduce the diffusion resistance as well as increase the amounts of electrolyte, reactant, product, and electron transfer [23,43]. Foam has various grades distinguished

by the number of pores, leading to differences in the specific surface area, mass transfer rate, and potential distribution. Meanwhile, graphene is a 2D carbon monolayer with a large specific surface area, chemical stability, high charge carrier mobility, and thermal stability. Although graphene is currently widely used in many applications, especially as electro-catalyst supports, graphene still has its drawbacks in fuel cells. Among graphene's weaknesses are extreme resistance and degree of deterioration due to the structural defects and strong planar stacking of the graphene sheets [35]. Graphite, on the other hand, is very fragile as it consists of different graphene planes linked by  $\pi$ -stacking interactions (where the theoretical spacing for the layer-to-layer carbon atom is 3.35 Å). Due to these problems, graphene foam (GF) with a 3D skeleton structure, namely, monolithic graphene films, became the focus. GF production using NF as a sacrificial template has reduced the strong  $\pi$ - $\pi$  interaction and inter-sheet resistance between the 2D graphene layers [29]. The large void volume, high porosity, and interconnected skeleton structure of GF leads to efficient mass, ion and electron transfer, and better electrolyte diffusion due to the low resistance at the catalyst interface [23,29,34,35].

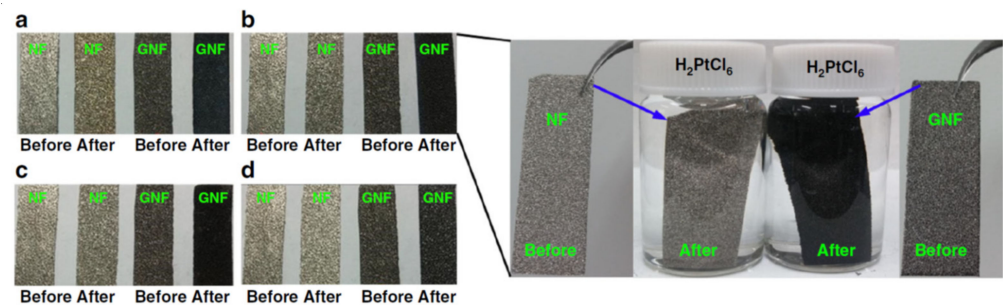


**Figure 1.** Optical photographs of NF and GNF before and after metal deposition in different electrolytes. (a–d) Comparison of NF and GNF before and after 1 h deposition in (a) 0.09 mM HAuCl<sub>4</sub> (pH = 4.2), (b) 0.09 mM H<sub>2</sub>PtCl<sub>6</sub> (pH = 4.5), (c) 0.9 mM AgNO<sub>3</sub> (pH = 5.3), and (d) 0.9 mM CuSO<sub>4</sub> (pH = 4.6), respectively. Reprint with permission from Ref [38]. Copyright 2018 Nature.

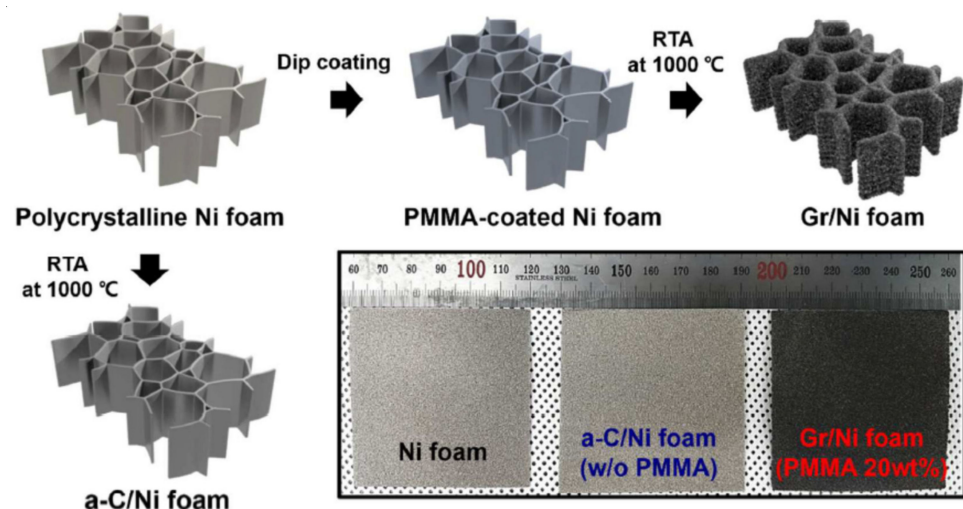


**Figure 2.** Schematic of the synthesis of a graphene film on Ni foam using the RTA process. Inset is photographs of a 6 × 6 cm<sup>2</sup> Ni foam sample before and after the growth of C-based films with/without the use of PMMA. Reprinted with permission from Ref [39]. Copyright 2018 Royal Society of Chemistry.

Powdery catalysts are commonly used in DLFCs that require the involvement of a binder to make the electrode slurry [44]. The presence of the binder decreases the electrochemical activity, as the binder reduces the ion and electron transport occurring in

the electrode and at the electrode/electrolyte interface [42] by blocking the catalyst active sites [20,45]. Therefore, the use of the 3D structured materials NF and GF can improve the performance when a binder is not required in the electrode [5,41,46–48]. 3D structured materials can also be used in place of conventional carbon cloth and carbon paper as supporting substrates [31,49] to reduce the poor catalyst use [50–52]. Besides, there are two types of phase boundaries in fuel cells, as shown in Figure 3; namely, a triple-phase boundary and a two-phase boundary [53]. A triple-phase boundary that has a liquid phase, an ion-conducting phase, or an electron-conducting phase causes specific problems related to the reactant-delivering pathway, proton-conducting pathway, and electron-conducting pathway, respectively. Alkaline fuel has been used to solve the triple boundary pathway problems and create a two-phase pathway. However, there are still inactive sites in the catalyst, as shown in Figure 3, that must be prevented, and using foam is one way of increasing the catalyst use. Besides, the electrodeposition effect of the catalyst in the inner and outer NF and GF must be considered, as mentioned by Verlato et al. [54], in which the authors stated that the inner foam is less effective than the outer foam. How the distribution and loading position of the catalyst plays an important role to increase or decrease the activity of the electrochemical reaction in DLFCs was examined.

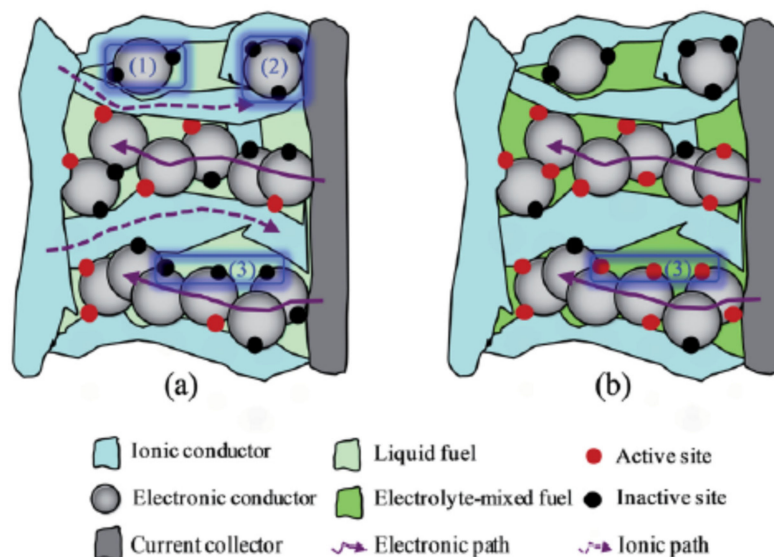


**Figure 3.** Schematic illustration of the catalyst layer and the regions (in red color) of (a) triple-phase boundary, and (b) two-phase boundary. Reprinted with permission from Ref [53]. Copyright 2014 Royal Society of Chemistry.

The use of NF and GF has significantly reduced carbon monoxide's (CO's) ability to be adsorbed on the surface catalyst while further enhancing the catalytic activity, stability, and durability of the electrochemical reaction in the fuel cell. The CO molecules on the catalyst surface are reduced by improving the particle distribution, thus increasing the number of catalytic active sites for the electrochemical reactions to occur [26]. However, how the mechanism of the electrochemical reaction occurs in DLFCs using NF and GF and to reduce CO adsorption and other poisonous intermediates on the catalyst surface remains a question. There must be some interaction between the catalyst and the support to reduce the adsorption energy of CO [26,28] and other poisonous intermediates [18] and further oxidize to complete the electrochemical reaction.

### 3. Current Achievement and Development of the Application of Nickel Foam and Graphene Foam in Direct Liquid Fuel Cells

#### 3.1. Methanol Electro-Oxidation Reaction

Pt is the best catalyst for the electrochemical reaction in DLFCs. However, the high cost and limited resources of Pt have led to several efforts to reduce Pt loading while maintaining the electrochemical reaction activity by methods such as alloying with other metals and using catalyst supports to increase the dispersion of the Pt catalyst [30]. Using layered double hydroxides (LDHs) that have an ionic solid surface is a new strategy created for achieving electrochemical conversion with a high chemical and thermal stability [55]. Ni(OH)<sub>2</sub> is used together with Pt metal as a catalyst, and NF is used as catalyst support for methanol oxidation reaction (MOR), as described by Yuan et al. [56]. Ni(OH)<sub>2</sub> can remove any poisonous intermediates during the MOR, and the large area provided by NF aided in the reactant and product removal, thus increasing the mass transfer coefficient. The Pt/NF and Pt-doped Ni(OH)<sub>2</sub>/NF materials show no oxidation peak during the CO-stripping voltammetry analysis, indicating that both catalysts have high resistance towards any poisoning effect. A catalyst with a very low Pt content and a co-catalyst with MoS<sub>2</sub>-Ni<sub>3</sub>S supported on NF is synthesized by Tang et al. [32]. During the CV scan in 1.0 M KOH, the hybrid catalyst Pt with MoS<sub>2</sub>-Ni<sub>3</sub>S has an electrochemical surface area (ECSA) of 76.7 m<sup>2</sup>/g<sub>Pt</sub>, which is higher than that of Pt/C, with a value of only 30.3 m<sup>2</sup>/g<sub>Pt</sub>. The ECSA value of the NF-supported catalyst is higher than that of the commercial carbon support because the Pt catalyst is highly exposed and uniformly distributed on the surface of MoS<sub>2</sub>-Ni<sub>3</sub>S with high porosity and surface area. Zhang et al. [30] deposited Pt on a NiCo-layer double hydroxide (NiCo-LDH) on NF to increase the anti-poisoning effect (by increasing the number of active sites for OH<sup>-</sup>) on the catalyst and stability. The stable support directly contributes to the high catalytic performance and tolerance observed during MOR. The ECSA value of Pt-NiCo-LDH/NF is 16 times higher than that of commercial Pt/C/NF; the ECSA values of Pt-NiCo-LDH/NF and commercial Pt/C/NF are 131.86 m<sup>2</sup>/g and 8.27 m<sup>2</sup>/g, respectively. Due to the advantageous high porosity of NF, Du et al. [57] produced a co-catalyst of CoSe/NiSe with a low loading of Pt, and XRD testing showed the presence of NiOOH/CoOOH on the catalyst surface. NiSe/NF helped improve water splitting and, in the presence of NiOOH/CoOOH, increased OH<sup>-</sup> adsorption, thus assisting in the oxidation of the CO that adsorbed on the surface of the Pt catalyst. This effect leads to a higher value of ECSA of 85 m<sup>2</sup>/g<sub>Pt</sub> when NF is used compared to Pt/C, which only has an ECSA value of 3.03 m<sup>2</sup>/g<sub>Pt</sub>.

Palladium (Pd) metal is a promising electro-catalyst that can catalyze the fuel oxidation in DLFCs and replace the Pt catalysts [12,54]. Niu et al. [58] investigated the effect of the precursor on the deposition of Pd on NF, as well as the arrangements and coverages of Pd by using a galvanic replacement method. A 2:1 atomic ratio of Pd to Ni results in an exposed NF surface, as shown in Figure 4, and leads to a catalytic interface composed of a Pd-Ni alloy or a bi-functional effect during the MOR, leading to a mass activity that is 1.5 times higher than that obtained with other ratios. Cheng et al. investigated the combination of Pd metal with MnO<sub>2</sub> for the MOR and the stability of the catalyst increases when the NF is used as the catalyst support [42]. The authors found that MnO<sub>2</sub> reduced the poisoning effect during the MOR, as Pd-MnO<sub>2</sub>/NF increases the current density by three times compared to the current density increase obtained with Pd/NF, while the NF helped to stabilize the catalyst, both of which increased the MOR activity. Yu et al. [6] have compared catalyst supports prepared with NF and with indium tin oxide (ITO) electrodes using Ag nanoparticles (AgNP) as the catalyst. AgNP/NF showed a better electrical conductivity than AgNP/ITO, as the interaction of Ag-Ni creates a new electron transfer pathway, and the NF helps to increase the electrolyte diffusion rate. In the stability test, the strong interaction between Ag and NF, which was determined using an ion implantation method, showed that the current density is in a stable condition, even after 5000 s. Then, Niu et al. [59] added Pd to form PdAg/NF for the MOR, and this combination was used to build a ternary alloy of Pd-Ag-Ni using a galvanic replacement

method. The atomic ratio of Pd:Ag plays an important role in increasing the mass activity by as much as 3.3 times the mass activity of the Pd/Ni binary alloy. Guo et al. [60] studied using the ion implantation method to dope Co nanoparticles (CoNPs) on NF to increase the electrical conductivity and mechanical stability of the catalyst-NF. Using this technique has increased the number of particle dislocations and defects in the CoNPs, thus increasing the number of active sites for the MOR. These factors, as well as using the free binder, have increased the mass activity and current density for the MOR.

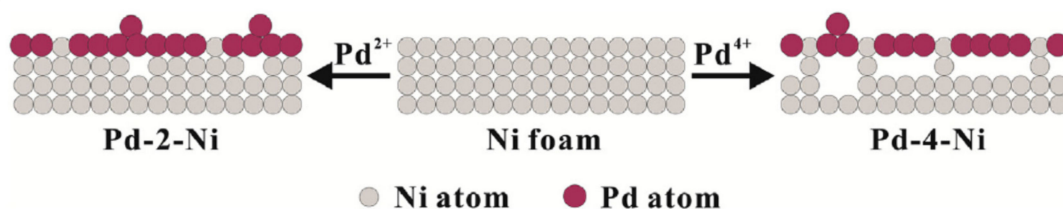


**Figure 4.** The formation of bifunctional catalyst Pd-Ni atom on NF for methanol electro-oxidation reaction by using the galvanic replacement method. Reprinted with permission from Ref [58]. Copyright 2016 Elsevier.

Jadhav et al. [61] used  $\text{MnCo}_2\text{O}_4$  as a catalyst grown on NF. The  $\text{MnCo}_2\text{O}_4$  material supported on the surface of NF formed a flake-like structure with a thickness of 20–22 nm. The NF increased the stability of the MOR by speeding up the ion/electron transfer rate, as proven in the stability test after 1000 cycles were performed. The current density reduced to 66% but increased back to 77% when the new electrolyte was replaced with an electrolyte containing the new methanol solution. The decrease in 66% is due to the consumption of methanol during the MOR. The Jadhav et al. group also used  $\text{MgCo}_2\text{O}_4/\text{NF}$  for the MOR [43], in which the Mg metal side adsorbed more  $\text{OH}^-$  than the NF side and further oxidized CO to  $\text{CO}_2$ . Meanwhile, Shi et al. [47] synthesized  $\text{ZnCo}_2\text{O}_4$  supported on NF using a solvothermal and calcination process. The duration of the solvothermal reaction used to form the grown catalyst sheets on NF affected the structure and porosity of  $\text{ZnCo}_2\text{O}_4$  and thus led to the surface area. The structure of  $\text{ZnCo}_2\text{O}_4/\text{NF}$  has been interlaced between the sheets of  $\text{ZnCo}_2\text{O}_4$ , making the diffusion of the electrolyte to the surface catalyst much easier. Not only that, but  $\text{ZnCo}_2\text{O}_4/\text{NF}$  also has high stability, even after the 1000th cycle in the CV analysis. The same  $\text{ZnCo}_2\text{O}_4/\text{NF}$  material was developed by Sreekanth et al. [46], but a different method was used to synthesize the catalyst at 180 °C and produce a cubic structure of  $\text{ZnCo}_2\text{O}_4$ . Another interesting study was carried out by Jadhav et al. [62], who developed mesoporous  $\text{ZnCo}_2\text{O}_3$  on NF. The same materials but with different morphologies still affected the electrochemical reaction in DLFCs [63,64]. Gu et al. [65] and Wang et al. [66] synthesized  $\text{NiCo}_2\text{O}_4$  nanosheets/NF and obtained an ECSA of 146.5  $\text{m}^2/\text{g}$  and 66.9  $\text{m}^2/\text{g}$  using different methods, respectively. Both materials have good stabilities, even after running the materials in an alkaline methanol solution after 500 and 1000 cycles.

The combination of other metals with cobalt oxide also resulted in a promising activity for the MOR and was supported on NF.  $\text{ZnCo}_2\text{O}_4$  and  $\text{NiCo}_2\text{O}_4$  supported on NF were synthesized by Tombac et al. [67] and showed a high current density, low onset potential, and strong stability. The temperature of the annealing process used to synthesize the catalyst with NF is very important, as increasing the temperature to more than 500 °C will change the NF to NiO. The formation of NiO reduced the active sites, thus reducing the reactivity of the MOR. The  $\text{MCo}_2\text{O}_4$  material formed nanoflower particles on the nanorod supported on NF. The anodic peak current density obtained using NF as support is higher than that obtained using the other materials such as glassy carbon, stainless steel mesh, and carbon. Both  $\text{ZnCo}_2\text{O}_4$  and  $\text{NiCo}_2\text{O}_4$  have current densities of 154  $\text{mA}/\text{cm}^2$  and 280  $\text{mA}/\text{cm}^2$ , respectively.

A powdery  $\text{Co}_3\text{O}_4$  material was derived from a zeolitic imidazolate framework-67 (ZIF-67) and supported on NF to form a 3D skeleton for MOR, and this binder-free process was performed by Qian et al. [44]. The combination materials have the characteristic mor-

phologies of a hollow structure, larger surface area, and high loading capacity. The hollow porous structure around  $\text{Co}_3\text{O}_4$  increases the mass transfer rate between the electrode and electrolyte as the electron resistance decreases as well as increases the number of active sites for adsorption and oxidation. Interestingly, the  $\text{Co}_3\text{O}_4$  supported on NF went through a pressure machine at a pressure of 10 MPa, but the catalytic activity remained the same after the pressure was introduced. Rajeshkhanna et al. [5] used a different precursor salt of  $\text{Co}_3\text{O}_4/\text{NF}$  to obtain  $\text{Co}_3\text{O}_4$  with different structures (micro-flowers, nanograss, and microspheres) as shown in Figure 5, surface areas, and MOR current densities, but the onset potential of  $\text{Co}_3\text{O}_4/\text{NF}$  was almost similar to that of  $\text{Co}_3\text{O}_4$ . The microspheres give the best performance and have a BET surface area and current density of  $100 \text{ m}^2/\text{g}$  and  $36.2 \text{ A/g}$ , respectively. In other different studies performed by Hassan et al. [68], mesoporous carbon was added on  $\text{Co}_3\text{O}_4/\text{NF}$ . The  $\text{C}/\text{Co}_3\text{O}_4/\text{NF}$  material exhibits a catalytic activity that was three times higher than that of  $\text{Co}_3\text{O}_4/\text{NF}$  and comparable current density retention during the stability test, which was performed with  $\text{NiCo}_2\text{O}_4$  with different catalyst supports.

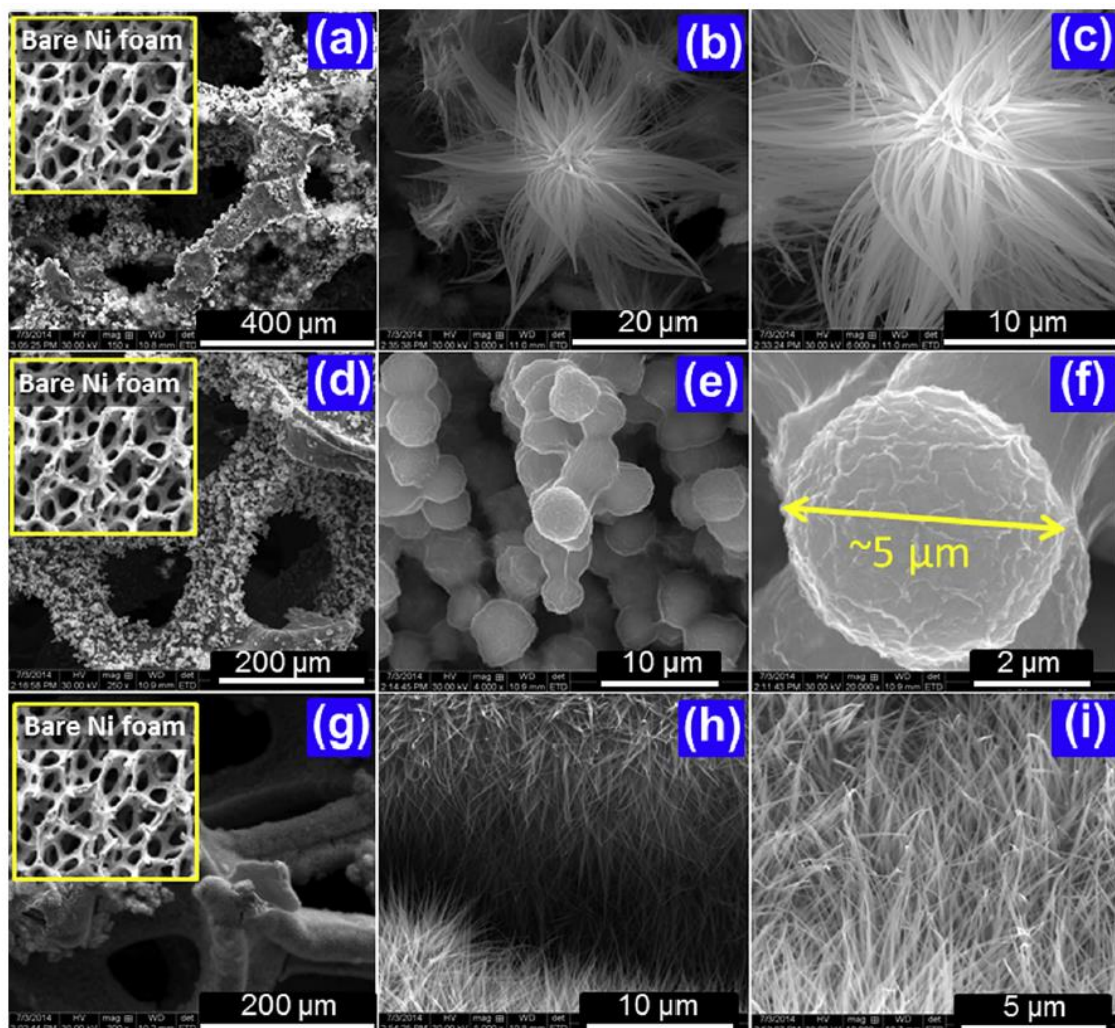


**Figure 5.** FESEM images of  $\text{Co}_3\text{O}_4$  grown on Ni foam under hydrothermal conditions using different anions, (a–c) microflower- $\text{Co}_3\text{O}_4$  with  $\text{Cl}^-$ , (d–f) microsphere- $\text{Co}_3\text{O}_4$  with  $\text{SO}_4^{2-}$ , and (g–i) nanograss- $\text{Co}_3\text{O}_4$  with  $\text{CH}_3\text{COO}^-$ . Reprinted with permission from Ref [5]. Copyright 2016 Elsevier.

Roy et al. [41] developed  $\text{CuO}/\text{NF}$  for the MOR through two processes, which are electrodeposition and calcination processes. The calcination temperature has been tested, and it was found that the temperature must not exceed  $450 \text{ }^\circ\text{C}$  to prevent the instability of NF and further transformation to  $\text{NiO}$ . The  $\text{CuO}/\text{NF}$  material showed a remarkably high

current density as well as a low onset potential and overpotential due to the easy pathways of electron tunneling from the NF. Roy et al. [69] developed a binder-free and carbon-free catalyst using  $\text{Co(OH)}_2/\text{NF}$  and compared the resulting catalyst with  $\text{Co}_3\text{O}_4/\text{NF}$  for MOR applications.  $\text{Co(OH)}_2/\text{NF}$  had an onset potential of the MOR that was much lower than that obtained by other researchers. The  $\text{Co(OH)}_2/\text{NF}$  materials have a high current density of 27 A/g due to the ability to control the intermediate kinetics at the electrode surface of  $\text{Co(OH)}_2/\text{NF}$ , being better than that of  $\text{Co}_3\text{O}_4/\text{NF}$ .

To increase the poison tolerance and long-term stability of catalysts used for MOR, Yuan et al. developed a core-shell of  $\text{Ni}_3\text{S}_2$  with many defects that were supported on NF [70]. The result showed that the increase in the stability, activity and poison tolerance is due to the electro-catalyst being supported on the NF without any binder, thus increasing the mass transport of electrons and ions. The stability test performed using cyclic voltammetry showed that the peak current is maintained, even after 5000 cycles were performed in 0.5 M KOH and 1 M methanol at a scan rate of 50 mV/s. Another nickel-based catalyst developed by Li et al. [36] used  $\text{Ni}_3\text{B}$  supported on NF. Usually, the Ni metal has a low activity towards the MOR, but not when using  $\text{Ni}_3\text{B}$  with a particle size of 100–200 nm. The mechanical stability obtained when testing in 6 M KOH with 0.5 M methanol was high, and it was shown that anodic oxidation efficiency can be maintained at 87%, even after 1000 cycles. Eisa et al. [20] developed Ni/NiO nanorods grown on the NF surface that has superhydrophilic surface characteristics. The strong attraction of water molecules is important so that the decomposition of methanol and water to form protons becomes easy [71]. Another synergistic effect catalyst of nickel oxide and nickel oxalate ( $\text{NiC}_2\text{O}_4$ ) was developed by Zhang et al. [48] and shown to have increased activity for MOR. The comparison of the MOR activity is very significant, as the current density of NiO/NF and NF is 34 mA/cm<sup>2</sup> and 14 mA/cm<sup>2</sup>, respectively. The current density value increased by three times when the methanol concentration was increased from 0.025 M to 0.40 M. Besides, Xiao et al. [72] and Luo et al. [73] synthesized different structures of NiO films and nanosheet@nanowire arrays on NF. Xiao et al. [72] used a NiO film/NF with high stability for the MOR, which resulted in the current retention decreasing to only 92% after the stability test was performed for 500 cycles.

Cheng et al. [74] used a combination of Ni and  $\text{CuS}_2$  with NF for the electrochemical conversion of methanol. The morphology resulting from the deposition of NiCu on NF is uniform, smooth, and compact but becomes a rough and uneven surface after sulphurization to form  $\text{NiCuS}_2$ . The addition of sulphide is performed to increase the electrocatalytic activity of the catalyst. The  $\text{NiCu}_2\text{S}_2/\text{NF}$  material has a high current density and a better catalytic activity and stability than  $\text{NiCu}/\text{NF}$ ;  $\text{NiCu}_2\text{S}_2/\text{NF}$  and  $\text{NiCu}/\text{NF}$  have current densities of 825 mA/mg and 673 mA/mg, respectively. Both electrodes can also maintain high stability after 5000 s, as the  $\text{NiCu}_2\text{S}_2/\text{NF}$  and  $\text{NiCu}/\text{NF}$  electrodes decay to only 76% and 74%, respectively. Hong et al. [75] investigated a hybrid NiO-CoO/NF material, in which the increase in the MOR activity is higher than that in pure NiO and CoO. However, the stability of the NiO-CoO/NF electrode decreased after 150 min, and the current density dropped from 110 to 85  $\mu\text{A}/\text{cm}^2$ .

Kung et al. [35] applied the GF as catalyst support for MOR by anchoring the PtRu catalyst on the GF surface to enhance the active surface area. The porous structure of GF allowed for the smooth mass transfer of the reactant towards the catalyst surface. The resistance to CO adsorption increased when the ratio of the current density of the forward scan to that of the backward scan increased, and thus, the long-term stability of PtRu/GF also increased. The present reduction observed after 900 cycles of CV, performed when using PtRu/GF, is only 0.73%. In comparison, the current density of PtRu/graphene and PtRu/C decreases significantly after 900 cycles to 55% and 79%, respectively. Yi et al. [34] used a high internal phase emulsion method to synthesize the GF (denoted as GF-HIPE) due to the low cost and simplicity of the method and ability to control the void size. A GF-HIPE that has an average void size of 146  $\mu\text{m}$  was used as a support for the PtRu nanoparticle catalyst. The high catalytic activity obtained using PtRu/GF-HIPE was due to the strong bonding

between the catalyst and support, as the surface of GF-HIPE contains many heteroatoms of nitrogen and oxygen to anchor PtRu. In addition to that, the large surface area and the existence of graphitic layers have reduced the charge transfer resistance during the MOR.

Zhang et al. prepared and used GF as catalyst support for Pt nanoflowers by a chemical vapor deposition (CVD) method [23]. The charge transfer resistance on the catalyst and GF showed a higher charge efficiency, thus giving a fast reaction rate, with a charge transfer resistance of  $11 \Omega \text{ cm}^2$ . This also suggested that the electron transport and ion diffusion achieved using GF is very effective. Another study by Zhang et al. [22] developed Pt nanoflower/GF materials for MOR. The GF has a larger surface area than commercial carbon supports, in which the surface areas of GF and commercial carbon supports are  $670 \text{ m}^2/\text{g}$  and  $250 \text{ m}^2/\text{g}$ , respectively. More of the Pt (111) crystal plane is exposed to the catalyst support due to the large surface area of the GF.

Cui et al. [12] synthesized a GF using a lamellar MCM-22 zeolite as a template and deposited Pd nanoparticles (PdNPs) for the MOR. The catalytic activity for the MOR increased very significantly by 1.7–2.9 times that of the commercial Pd/C catalyst. The ECSA value of Pd/MGF is  $59 \text{ m}^2/\text{g}$ , while that of Pd/C is only  $46 \text{ m}^2/\text{g}$  due to the better dispersion of ultrafine PdNPs on the GF surface. Cheng et al. [29] grew a binder-free 1D cobalt sulphide nanoneedle catalyst on the GF surface. The binder-free method prevents the self-aggregation of the graphene surface on the interconnected structure of the GF. Indirectly, the binder-free method increases the catalytic activity of the site, improves the interfacial contact, reduces the resistance, and increases the transfer efficiency.

Some studies use deposit graphene on the NF surface without sacrificing the NF. Studies that used both graphene and the NF produce graphene that is highly stable in acidic/alkaline media, low cost, and has a high electronic conductivity [76]. Wang et al. deposited a graphene hydrogel in NF (G-NF), which was used as a support catalyst for Pt in MOR [45]. The rate of the MOR achieved with rGO-NF is 27 and 86 times higher compared with that achieved with glassy carbon and Pt electrodes, respectively. The poisoning effect obtained using G-NF is very low, and the  $I_f/I_b$  ratio is high, with a value of 18.2. Yu et al. [77] investigated using the combined G-NF material as a support for  $\text{NiCo}_2\text{O}_4$  catalysts used for MOR. The 1D  $\text{NiCo}_2\text{O}_4$  nanoneedles grown vertically on the graphene surface have features including a high capacitance, with a value of  $1588 \text{ F/g}$  at  $1 \text{ A/g}$  and are suitable for use as the current collector in DMFCs and other types of DLFCs. Thoufeeq et al. [78] studied nickel-GF (Ni-GF) prepared by a modified polyol method for use in MOR. The authors state that the activity of Ni in the electrochemical reaction is highly dependent on the structure and preparation method of Ni. There is no NiO present on the surface of Ni-GF, which has a highly stable current density as high as  $4.81 \text{ mA/cm}^2$ , as determined by chronoamperometry analysis, which is 1.7 times higher than that of pure Ni.

Gao et al. used graphene oxide-NF as a conductive substrate for the polyoxometalate encapsulation of Pt (PPt/GO-NF) [76]. The functional groups that exist on the graphene surface prevent the mobilization of Pt nanoparticles, while polyoxometalate is used to increase the electronic transfer capacity and size of the Pt nanoparticles. The PPt/GO-NF material prevents the CO adsorption effect by having an  $I_f/I_b$  ratio of 5.10 and a maximum mass activity at  $250.6 \text{ mA/mg}$ . Kamyabi et al. [24] investigated combining Pt and NiO with graphene oxide (GO), which were supported on NF. NiO and GO were synthesized by using a hydrothermal method, while the Pt is electro-deposited on the NiO-GO surface. The ratio of the forward scan and backward scan ( $i_f/i_b$ ) during the MOR is important for determining the poisoning degree of the catalyst. In comparison with other supports, such as CNF and nanowires, which have  $i_f/i_b$  ratios of 1.1 and 1.22, NF showed a poisoning tolerance, with an  $i_f/i_b$  ratio of 1.05. Pure Ni is used in MOR as  $\text{NiOOH}$ , which becomes the determining step, while pure copper (Cu) tends to transform to  $\text{Cu}(\text{OH})_2$  and  $\text{CuO}$ , in which both materials result in positive outcomes in MOR. Catherin Sesu et al. [79] developed both combinations of Ni-Cu to form a 3D structured material of a Cu-Ni-rGO

foam for MOR. The current density of Cu-Ni-rGO foam can retain value as high as 95% after operation for 600 s.

The gas diffusion layer (GDL) usually used in fuel cells is carbon paper and carbon cloth. The exploration of using stainless steel fiber felt (SSFF) and metal foam as the GDL has become more extensive. Zhu et al. [80] tested the use of GF as the GDL in a micro-DMFC. The fiber size is larger in GF than in the carbon paper, and the contact resistance decreased to as low as 0.259  $\Omega$ . The new GF as the GDL instead of carbon paper have also resulted in increasing the power density from 25 mW to 31.2 mW due to the shorter diffusion path of methanol toward the catalyst surface.

### 3.2. Ethanol Electro-Oxidation Reaction

Ethanol produced from abundant and renewable agricultural products and biomass substrates has been applied to DLFCs [37]. Pd metal and Pd-based metals have high catalytic activity and are more abundant, less expensive, and less poisoning than Pt during the ethanol oxidation reaction (EOR) in DLFCs [33,81]. Wang et al. [82], Mikolajczyk et al. [37], Li et al. [53], Pierozynski et al. [40], and Verlatto et al. [54] used different preparation methods to support Pd metal on NF to form a 3D structured catalyst. Pd/NF has a large surface area and produces a higher ECSA than the Pd film electrode, Pd/C, and Pd bulk catalyst. The developed Pd/NF material is also durable and has a catalytic activity that is eight times higher than that of the Pd film [82]. Li et al. [53] developed a thin and porous Pd sponge structure on an interconnected NF structure, with few aggregates forming. There are three advantages of this method, which were discovered by the authors, in terms of the catalytic activity of the EOR: the increased ECSA, reduced loss of chemical precursors, and more uniform Pd-sponge structures on NF. Mikolajczyk et al. [37] and Pierozynski et al. [40] investigated using Pd/NF for EOR and their effect when the reaction temperature was changed (20–60 °C). As the temperature increases, the current density also increases, and the oxidation potential tends to move towards more positive potentials. Meanwhile, Verlatto et al. [54] found that the factors of the concentration and the duration of the electrodeposition method have changed the size of Pd, thus leading to different mass densities for EOR, including reactions with other alcohols, such as methanol, ethylene glycol, and glycerol. The surface of NF is modified by replacing the pure nickel with hydroxide to reduce the poisoning of carbonaceous adsorption on the Pd surface and further increase the oxidation rate of the reaction. However, Chen et al. [83] found that the morphologies and growth rate of the modified Ni(OH)<sub>2</sub> material greatly affects water dissociation and results in the high insulating property of hydroxide, which will lower the electron conductivity of the materials.

Other than Pd and Pd-based metal, Pt and Pt-based metal were also tested to improve the EOR developed by Pierozynski et al. [84,85], which used Pt/NF [84] and PtSn/Ni(OH)<sub>2</sub>/NF [85]. Sn was added to PtSn/Ni(OH)<sub>2</sub>/NF to prevent the dissolution of Pt during the electro-oxidation reaction. Although Pt formed and was non-uniformly distributed on the NF surface, the charge transfer resistance of the /Ni(OH)<sub>2</sub>/NF was lower than that of Pt/NF. The advantages of the Sn in PtSn and the hydroxide layer on NF have increased the reactivity of the EOR and reduced the charge transfer resistance in the catalyst. The slow rate of the EOR achieved using nickel led to the study by Hatamie et al. [86], which compared the EOR resulting from using NF and Au/NF. The performance of Au nanoparticles with an average size of 37 nm increased by 253% relative to that of NF. The authors also studied the effects of the concentration of ethanol and mixing rate, but the mixing rate did not affect electro-oxidation, because the diffusion-controlled processes are not effective. Although other studies showed that the rate of the reaction using NF was slow, Zhang et al. [48] and Eisa et al. [20] used NiO/NF and Ni nanorods (NNR)/NF, which show a high reactivity for the EOR, respectively. The NiO derived from the NiC<sub>2</sub>O<sub>4</sub> precursor and the presence of NiC<sub>2</sub>O<sub>4</sub> on the NiO/NF surface have advantages because the presence of NiC<sub>2</sub>O<sub>4</sub> improves the cycling performance and specific capacitance [48]. While, the small size of the nanorod morphology, with the wettability and hydrophilic

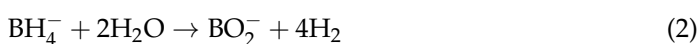
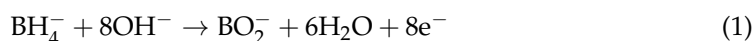
properties of the NNR surface, has increased the surface area by 18 times compared to the surface area of NF [20].

Kung et al. [35] have used PtRu/GF, which had a higher EOR reactivity than other catalyst supports, such as graphene, carbon black and PtRu without a support. In terms of the stability, GF has a higher stability than PtRu/graphene after being tested in the stability cycle. Xu et al. [87] have emphasized the importance of obtaining the monolithic 3D GF structure, which helps to enhance the EOR performance of PdCo alloy and other metal and metal oxide catalysts. This is because developing the GF using NF as a template will lower the volume and specific surface area of GF and lead to a low volumetric loading and energy capacity. The monolithic 3D GF can be produced using the chemical vapour deposition (CVD) method. Liu et al. [88] used carbon foam (CF), used as a support on Pt skin and PtCo nanowires, to prevent the Ostwald ripening of Pt and dissolution and aggregation of the nanoparticles during the electro-oxidation reaction in fuel cells run for a long time. Li et al. [81] produced PdNi/CF with various atomic ratios of Pd:Ni. XPS revealed that the presence of NiO from the PdNi alloy has helped to increase the EOR rate in alkaline media. There have been numerous studies showing the high reactivity of NiO in EOR. Authors have also suggested that PdNi/CF can be used as a direct electrode in DEFC without using conventional carbon paper or carbon cloth.

Zhang et al. [89] argue that using GF-NF provides several advantages over using the CVD method to produce GF. Combining solution casting and electrochemical reduction methods gives the advantage of the synergistic interaction of nickel-Pd, which enhances the EOR. Tsang et al. [90] deposited a graphene aerogel (GA) on NF, found that an increase in the Pd loading from 0.8 wt.% to 7.65 wt.% increased the EOR rate and obtained an  $I_f/I_b$  ratio of 2.72. Based on the potential demonstrated by GA/NF, the Tsang group [91,92] added Pd to the PdPt alloy and applied the current-collector-free electrode into the DEFC. The power density generated using the PdPt alloy is 3.6 mW/cm<sup>2</sup> at room temperature. At 60 °C, the performance of the single cell DEFC was tested by Sun et al. [49] using an ultra-low loading Pd/C-NF, with a value of 202 mW/cm<sup>2</sup>. Jiang et al. [33] produced a Pd distribution on GNF using a metal atomic layer deposition technique and found that an ultra-low Pd loading (50 µg/cm<sup>2</sup>) in GNF increased the current density by 2.64 times compared to the current density of a commercial Pd catalyst. This technique has the advantage of controlling the atomic layer thickness, which can lead to highly dispersed nanoparticles. In addition, Doğan et al. [93] deposited Pd on the reduced graphene oxide (rGO) at the NF surface, also resulting in remarkable activity that was comparable to that achieved by researchers using GNF as the catalyst support.

### 3.3. Borohydride Electro-Oxidation Reaction

Borohydride (NaBH<sub>4</sub>) is used as a fuel in DLFC because it has many hydrogen carriers. The specific capacity of NaBH<sub>4</sub>, with a value of 5.7 Ah/g, is higher than that of methanol, and NaBH<sub>4</sub> also has other advantages, which include its high gravimetric energy density (7100 Wh/kg), high volumetric energy density (7314 Wh/L) and high cell voltage (1.64 V). The electro-oxidation of NaBH<sub>4</sub> (BOR) does not cause problems, such as catalyst poisoning, does not release CO<sub>2</sub>, is non-flammable, and possesses many hydrogen carriers. Catalyst poisoning did not occur because no carbon element was involved in the BOR. The complete oxidation of BOR produces 8-electrons, as shown in Equation (1), but the hydrolysis of NaBH<sub>4</sub> also occurs concurrently, as shown in Equation (2). However, the main problem with the BOR is the conversion efficiency, and the selectivity requires that a catalyst can reduce the hydrolysis reaction that occurs in the BOR [94].



Yang et al. [50] synthesized Au nanosheets (AuNSs) and nanoparticles (AuNPs), which were to be supported on NF. The catalytic activity of the outstanding AuNS/NF

material was 278% higher than that of AuNP/NF, and also, the  $H_2$  gas produced by AuNS/NF diffused freely without blocking the active surface sites, thanks to the high porosity of NF. Song et al. [51] synthesized the nanosheets of PtCo/ $Co_3O_4$  on the NF surface. The presence of Co metal and  $Co_3O_4$  make it easy to break the B–H bond in the BOR. Due to the advantages of Co metal breaking the B–H bond, Guo et al. [95] produced a low cost Ni-Co alloy/NF to further enhance the catalytic activity of the BOR as a result of the synergistic effect of Ni-Co. Song et al. [31] synthesized nanoneedles of ternary Pd alloys on NF by increasing the amount of CuNi to reduce the cost of loading the Pd catalyst without reducing the catalytic activity of BOR. Altering the pure electronic conductivity of the Pd metal and the unique structure of the NF and nanoneedles have resulted in an activation energy and number of transferred electrons during the BOR of 18.42 kJ/mol and  $4.9 e^-$ , respectively. Ma et al. [94] found that the fuel conversion efficiency in DBFCs was dependent on the catalytic activity. In addition, the  $CoSn_x$ -B/NF catalyst developed by Ma et al. [94] also demonstrated the importance of the Co:Sn ratio in influencing the power density, which increased by 1.58 times compared to the power density of Co-B/NF (only  $100 mW/cm^2$ ).

Santos et al. [96] and Gouveia et al. [97] used various metal foam for applications in DBFCs. Santos et al. [96] used Ni-Cu foam to increase the amount of  $BH_4^-$  oxidized per unit volume and subsequently improved the single cell performance of a DBFC. Gouveia et al. [97] states that Co metal tends to promote the hydrolysis reaction, while the Ni metal is more preferable to proceeding with the BOR pathway. In addition, the research proved that the atomic ratio of Ni, Cu, Co and Fe in the foam plays an important role in DBFCs, either to proceed with the BOR or the hydrolysis reaction. As shown by Santos et al. [96], a certain Ni-Cu atomic ratio showed that the BOR is the preferred reaction pathway in DBFCs. However, the Li et al. group [98–100] used Co-based and Au-based catalysts deposited on reduced-graphene oxide foam (rGoF), in which all the catalysts reacted by a first-order reaction. Pure Au/rGoF [98] as shown in Figure 6 has a high electron transfer rate, with value of  $7.2 e^-$ , because pure Au/rGoF has a lower activation energy and smaller charge transfer impedance than CoAu/rGoF [100] and CoNi/rGoF [100], in which the electron transfer is only  $6.9 e^-$  and  $6.7e^-$ , respectively.

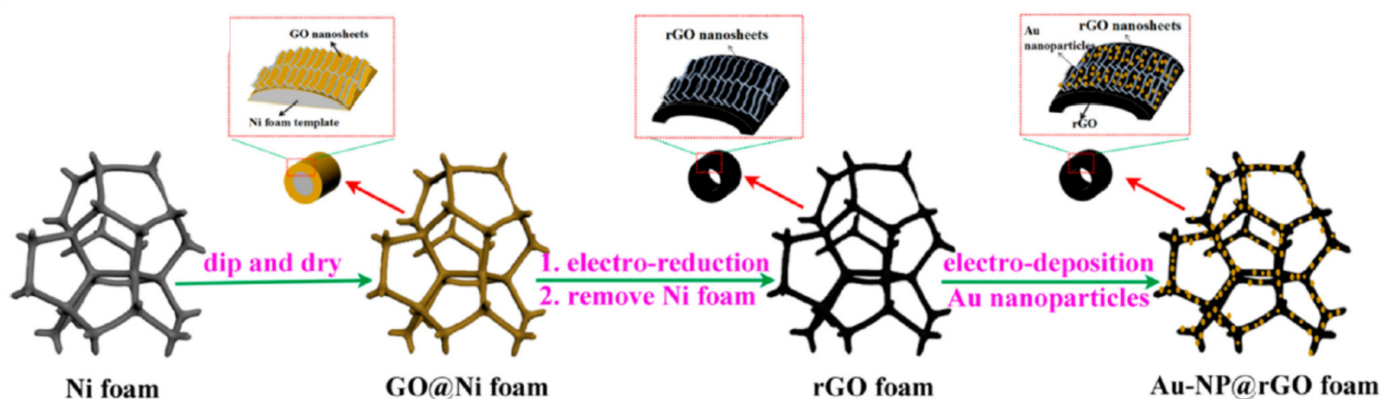
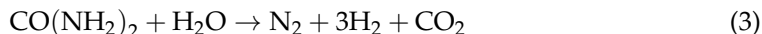


**Figure 6.** Flowchart of the preparation of Au-NP@rGO foam electrode. Reprinted with permission from Ref [98]. Copyright 2019 American Chemical Society.

### 3.4. Urea Electro-Oxidation Reaction

Urea ( $CO(NH)_2$ ) has advantages as a fuel in DLFC, as it is abundant and low cost, has high energy density, is non-flammable, is a harmless product of electro-oxidation in DLFCs (nitrogen and carbonate), is non-toxic, and has a lot of hydrogen carriers [101,102]. A fuel cell that uses urea as a fuel is called a direct urea fuel cell (DUFC) [48], while the cathode of DUFCs that uses hydrogen peroxide ( $H_2O_2$ ) as the oxidant is called a direct hydrogen peroxide fuel cell (DUPFC) [102]. The urea can be obtained from fertilizer, wastewater, and urine, which can be applied as fuel in DUFC [101,102]. The advantages of the DUFC

can not only produce the hydrogen gas but also can reduce the water pollution [103] and can be applied as a spaceship power source [102]. However, a major problem with the urea electro-oxidation reaction (UER) is the sluggish reaction kinetics [104], and thus, an efficient, stable, and low cost catalyst is needed [105].



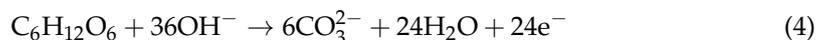
Guo et al. [101] supported a Ni-Co alloy with different ratios as low as 0% Ni and as high as 100% on NF for the urea electro-oxidation reaction (UER) in DUFCS. Ni-Co/NF is tested on a DUFCS, and among the factors that play a role in achieving the best single DUFCS performance at a temperature of 70 °C, with a performance output of 31.5 mW/cm<sup>2</sup>, are the urea concentration, operation temperature, and flow rate. The authors also tested pure human urine, but the power output was as low as 7.5 mW/cm<sup>2</sup>, which is lower than the power output of artificial urea, with a value of 17.4 mW/cm<sup>2</sup>, due to the various chemical compounds in human urine. Qian et al. [106] used the unalloyed state of Ni-Rh supported on NF, in which the presence of Rh that reduces the poisoning at the Ni surface and facilitates the UER. However, the authors also stated that the adsorption of CO<sub>2</sub> on Rh is still unknown.

Ye et al. [102] developed LDH on the Ni surface on the NF by controlling the temperature reaction to reduce the usage of noble metal catalysts. The rate of hydrogen bubbling during the UER is fast and produces a power density as high as 19.7 mW/cm<sup>2</sup> at a temperature of 20 °C. In addition, the synergistic effect of metallic NF with the many defects of Ni(OH)<sub>2</sub> from the Ni<sup>2+</sup> ions and oxygen vacancies, as prepared by Yan et al. [107], showed the long-term stability of the UER. Tang et al. [105] added Se on the LDH Ni and investigated the nanowire structure of Se-Ni(OH)<sub>2</sub> on the NF surface. The addition of Se as well as the LDHs to create more active sites reduces the amount of CO<sub>2</sub> adsorbed/desorbed. The synergistic effect on both metals has further increased the reaction kinetics. Zhang et al. [48] developed low cost NiO/NF by a chemical bath deposition method to prevent the formation of non-active sites for UERs. Zhan et al. [108] controlled the height and thickness of NiO nanowalls (NiO-NW)/NF by changing the amount of ammonia fluoride. The morphology of the NiO-NW/NF material affects the reactivity and stability in which the NiO-NW/NF is produced in the presence of ammonia fluoride is stable even after 12 h, while the NiO-NW/NF that prepared without ammonia fluoride is not stable after 12 h. To improve the electronegativity of Ni, Sha et al. [104,109] synthesized efficient NiCo<sub>2</sub>S<sub>4</sub> nanowire catalysts on NF, resulting in a low onset potential and high activity during the UER as well as an NF with good stability and high electronic conductivity. The increased activity is due to the many active sites on Co with a high-density defect structure.

### 3.5. Glucose Electro-Oxidation Reaction

Glucose is renewable fuel energy generated from agricultural activity. The application of glucose in DLFCs has advantages; for instance, glucose has a high theoretical energy density (4430 Wh/kg) and is abundant in nature, easy to handle and produce, non-toxic, and cheap. Glucose is also used in enzymatic and microbial fuel cells, in which these fuel cells use enzymes and microorganisms to break down the bonds in glucose, respectively. The main problem with using microorganisms as the catalyst is the sluggish reaction kinetics of the glucose electro-oxidation reaction (GluOR) and difficulty transferring the electrons from the catalyst surface to the electrode surface. Meanwhile, using enzymes is highly costly, has a limited lifetime and limited stability, and only reacts with partial electro-oxidation. These deficiencies lead to the application of direct glucose fuel cell (DGLuFC), and subsequently, producing an efficient catalyst is a challenge to reduce the sluggish fuel oxidation reaction kinetics, substrate crossover, and low catalytic activity for the GluOR due to the high concentration of hydroxyl ions and reaction intermediates [110,111].

Equation (4) showed the GluOR at the anode side, in which a total of 24 electrons were generated, but usually, the GluOR can only harvest two electrons.

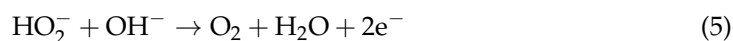


Chen et al. [112] used Ag metal as a catalyst, and NF acted as catalyst support and an electrode in the DGFC. The 3D NF with a high porosity facilitated the diffusion of glucose, which has a larger molecular structure than other fuels used in the DLFC. This study found that heating the electrolyte increased the performance of the DGluFC by 2.03 mW/cm<sup>2</sup> at 80 °C. The problem of slow electron transfer during the glucose electro-oxidation reaction (GER) has led to the use of methyl viologen and NF by Liu et al. [110] as an electron mediator and electrode, respectively. However, Yang et al. [111] also used the same electron mediator and electrode and tested them in a DGluFC with different operating conditions, such as different types of membranes, concentration mediators, KOH, and glucose. Varying all the factors has resulted in the optimum performance of the DGluFC at 25 °C with 5.20 W/cm<sup>2</sup>. Li et al. [113] investigated the different types of mediators with the NF as the electrode. The mediators used in this study were anthraquinone (AQ), methyl viologen (MV), neutral red (NR), methylene blue (MB), 2-hydroxy-1,4-naphthoquinone (NQ), and 1,5-dichloroanthraquinone (DA). The NQ mediator showed the highest performance, with a peak power density of 16.10 W/m<sup>2</sup>, with advantages of lower toxicity and high catalytic activity in GluOR. Chen et al. [114] tested the various operating parameters of the DGluFC using Au/NF and identified the role of the temperature, concentration glucose, KOH and medium to obtain a power of as high as 26.6 mW/cm<sup>2</sup>.

Tsang et al. [115] investigated by applying a graphene aerogel on NF (GE-NF) as a catalyst support for Pd-Pt alloys with different Pt:Pd ratios. A Pt:Pd ratio resulted in a high performance at 1.25 mW/cm<sup>2</sup> with a total loading of only 8.13 wt.%, which is a better performance than observed in other studies using high metal loading and carbon as the catalyst support. Zhao et al. [116] used Ni-rGO/NF and compared it with an NQ mediator/activated carbon. The results suggest that Ni-rGO/NF is an alternative to costly NQ and Ni-rGO/NF and can enhance the OCV of the single DGluFC. Wu et al. [117] added ZnO to the G-NF support to increase the sensitivity and selectivity for glucose detection and the initiation of the GluER. Wu et al. detected glucose at concentrations as low as 5 μM with a sensitivity of 129.44 μA/mM.cm<sup>2</sup>. Thoufeeq et al. [78] also tested the glucose sensitivity using rGO-NF, but rGO-NF only detected concentrations as low as 10 μM. In addition to NF and GF, copper foam [118] was used with metal-doped-Cu<sub>2</sub>O for GluORs. Cu nanoparticles that have a low mechanical stability and durability have led to the use of CF by El-Nagar et al. [119]. The metals used with 4% loading are nickel, cobalt, and iron and are doped on the surface of Cu<sub>2</sub>O. The number of active sites of Cu<sup>3+</sup> is increased after the deposition of nickel, cobalt, and iron atoms.

### 3.6. Hydrogen Peroxide Electro-Oxidation and Electro-Reduction Reaction

Hydrogen peroxide (H<sub>2</sub>O<sub>2</sub>) is used as a fuel in DLFC because it has the advantage of being an energy carrier, being carbon free and having a low cost as well as being workable without water. The H<sub>2</sub>O<sub>2</sub> electro-oxidation reaction (H<sub>2</sub>O<sub>2</sub>OR) is fast, does not poison the intermediate at the anode side, as shown in Equation (5), and does not need the costly Pt catalyst. However, a strong oxidant such as H<sub>2</sub>O<sub>2</sub> requires a very stable catalyst such as a noble metal [120]. In addition, the binder gradually degraded in the harsh environment of H<sub>2</sub>O<sub>2</sub> and KOH and needs the strength and high mechanical stability of catalyst support. The concentration of H<sub>2</sub>O<sub>2</sub> also needs to be studied, because the use of H<sub>2</sub>O<sub>2</sub> leads to chemical decomposition in DLFC.



The strong oxidant of H<sub>2</sub>O<sub>2</sub> is suitable to be used in DLFC at the cathode side for the H<sub>2</sub>O<sub>2</sub> electro-reduction reaction (H<sub>2</sub>O<sub>2</sub>RR), as shown in Equation (6), due to its advantages:

$\text{H}_2\text{O}_2$  is easier to store and handle than gaseous oxygen and fast reduction reaction kinetics. The high energy density and cell potential [120,121] increased the theoretical cell voltage of DLFC [122,123] due to the electrochemical reaction having a lower activation barrier than  $\text{O}_2$  [120,124] and no intermediate by-products. The  $\text{O}_2$  bubbles that form after the  $\text{H}_2\text{O}_2\text{RR}$  need to efficiently diffuse without impeding the electrochemical reaction. Therefore, NF and GF are seen to better help reduce these problems than the use of carbon cloth and carbon paper [52].



Song et al. [120], Yang et al. [121,125], and Xiao et al. [122] investigated the  $\text{H}_2\text{O}_2\text{OR}$  using Ni micro-particles supported on NF. Ni can produce LDHs on the Ni surface give a power density of  $19.4 \text{ mW}/\text{cm}^2$  at  $20^\circ\text{C}$  using  $\text{H}_2\text{O}_2$  instead of oxygen gases. The function of  $\text{Ni}(\text{OH})_2$  on the catalyst surface helps to break the  $\text{H}_2\text{O}_2$  bond, and their mechanism is presented as shown in Figure 7. Xiao et al. [126] used  $\text{NiCo}_2\text{O}_4/\text{NF}$  for  $\text{H}_2\text{O}_2\text{OR}$  and hydrogen peroxide electro-reduction reactions ( $\text{H}_2\text{O}_2\text{RR}$ ). Controlling the immersion time and electrodeposition time can produce various morphologies, such as nanowires, nanothorns, and nanohoneycombs, on the NF surface. The different interaction between the valence electrons of Ni and Co resulted in the current density being as high as  $520 \text{ mA}/\text{cm}^2$  and  $330 \text{ mA}/\text{cm}^2$  for the  $\text{H}_2\text{O}_2\text{OR}$  and  $\text{H}_2\text{O}_2\text{RR}$ , respectively. Cheng et al. [127] also applied the  $\text{Co}_3\text{O}_4$  with various crystal sizes and morphologies on the NF surface by a simple solvothermal method and used for  $\text{H}_2\text{O}_2\text{RR}$ . The good conductivity achieved using ultra-fine nanowires  $\text{Co}_3\text{O}_4$  is due to the short transfer path of the electrons.  $\text{SnO}_2$ , which has intriguing properties, such as good chemical properties, high electron mobility, and low cost, is applied by Sun et al. [124] on the NF surface. The well-known Pd metal, which has a high catalytic activity and stability in the harsh environment of  $\text{H}_2\text{O}_2$ , is used as a catalyst and deposited on the  $\text{SnO}_2$  surface. One main disadvantage of  $\text{H}_2\text{O}_2$  is easy to decompose the DLFC components, and thus, a low concentration of  $\text{H}_2\text{O}_2$  is used in the  $\text{H}_2\text{O}_2\text{RR}$ . However, the high mechanical stability and activity of Pd/ $\text{SnO}_2$ -NF are unaffected, using a high concentration of  $\text{H}_2\text{O}_2$ .

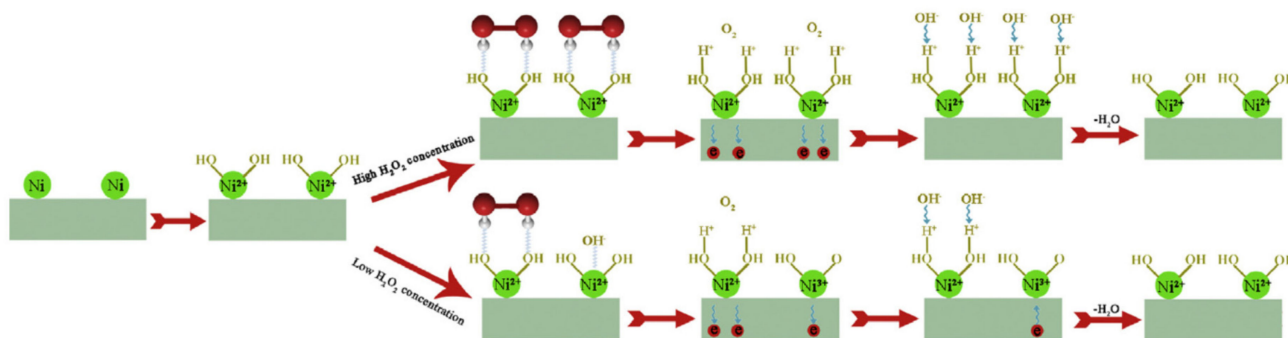


**Figure 7.** Schematic diagram depicting the mechanism for the  $\text{H}_2\text{O}_2$  electrooxidation on the Ni/Ni-foam electrode. The red and silver circles refer to the oxygen and hydrogen atoms in  $\text{H}_2\text{O}_2$ . Reprinted with permission from Ref. [125]. Copyright 2013 Elsevier.

Another combination of both rGO and NF was prepared by Song et al. [120] through a hydrothermal method and used as Pd catalyst support in a DLFC. Fast electron transfer occurs due to the plentiful channels for  $\text{H}_2\text{O}_2$  diffusion in the rGO-NF, and the electrons reached the Pd surface. Pd/rGO-NF produced a low activation barrier for the  $\text{H}_2\text{O}_2\text{RR}$ , with a value of  $8.202 \text{ kJ}/\text{mol}$ . Ye et al. [52] used a carbonization method to produce a carbon foam from polyurethane foam. Co and Pt metals are used to prepare a binary alloy catalyst by an electrodeposition method and a chemical deposition method to achieve  $\text{H}_2\text{O}_2\text{RR}$ , respectively. The high use of a catalyst leads to high catalytic performance and the quick release of the produced bubbled gas derived from the carbon foam.

### 3.7. Other Electro-Oxidation Reaction in DLFC

Other DLFCs have shown promising and rapid research development in electro-catalysts. However, the use of NF and GF as catalyst supports for electro-oxidation in direct glycerol fuel cell (DGFC), direct ethylene glycol fuel cell (DEGFC), direct hydrazine fuel cell (DHFC), and direct ammonia fuel cell (DAFC) is still limited. Cui et al. [12] used ultra-small Pd/GF for glycerol and ethylene glycol electro-oxidation reactions in DLFC. Ultra-thin nanosheets of graphene were formed on the MCM-22 zeolite as a template. The resulting mass activity showed the effect using GF as a support, with a value of 4.056 A/mg<sub>Pd</sub>, while the carbon support produced a value of 1.438 A/mg<sub>Pd</sub> in the ethylene glycol electro-oxidation reaction. Shih et al. [128] investigated Ni(OH)<sub>2</sub>/NiOOH supported on NF for the ammonia electro-oxidation reaction in a DLFC. Two challenges need to be addressed in ammonia electro-oxidation are the dimerization reaction and the complicated selectivity caused by the multiple electron transfers. To increase the selectivity, Shih et al. [128] used Ni(OH)<sub>2</sub>/NiOOH/NF as an anode with the consideration of several factors, including the pH of the solution, temperature, current density, and initial NH<sub>3</sub>-N concentration. The result showed that the presence of Ni in the anode made the oxidation reaction process from NH<sub>3</sub> to NO<sub>3</sub><sup>-</sup> and N<sub>2</sub> easy. Nickel-phosphate nanowires (NP) were grown on NF, as developed by Wen et al. [129] through a one-step phosphorization method for direct hydrazine fuel cell (DHFC). The NP/NF material is modelled using a first-principle calculation, which showed that the NPs have a high density of active sites and an electrical conductivity due to the addition of phosphate atoms, thus increasing the number of active sites and improving the morphology of the nanowires, respectively. Feng et al. [130] then alloyed the Ni metal with Zn and formed a nanosheet of Ni-Zn supported on NF for DHFC. The complete electro-oxidation of hydrazine produced a 4-electron pathway, and Ni-Zn/NF was 100% selective for the complete hydrazine electro-oxidation reaction.

Table 1 showed the summarized application of NF and GF as catalyst supports and their performance in DLFCs. This table shows the types of metal that have been used and supported by nickel foam and graphene foam. The reaction medium plays an important role in increasing the rate of the electrochemical reaction. Resistance to catalyst poisoning can be measured through a ratio of I<sub>f</sub>/I<sub>b</sub> value where a high value indicates the catalyst can reduce catalyst poisoning. Not all catalysts are tested in a single cell performance test, but almost all catalysts supported by NF and GF show good stability and durability after being tested for a long time.

**Table 1.** The summarized application of NF and GF as catalyst supports and their performance in DLFCs.

Foam	Catalyst	Fuel Concentration (M)	Medium	Onset Potential, Oxidation Potential, Current Density	$I_f/I_b$ , Mass Activity	ECSA/Surface Area, Charge Transfer Resistance ( $R_{ct}$ ), Electron Transfer	Activation Energy, Power Density	Stability, Durability and Other Information	Ref.
NF	Pd	0.5 M Methanol	1.0 M KOH	-	Mass activity = 650 A/g	-	-	-	[54]
NF	Pd	1.0 M Methanol	1.0 M NaOH	Onset potential = -0.562 V (vs. Ag/AgCl); Oxidation potential = -0.047 V (vs. Ag/AgCl)	Mass activity = 180.8 mA/mg	Electron transfer = 6	-	The catalyst still maintain 86% of the activity after 200 cycles	[58]
NF	Co	50 mM Methanol	1.0 M NaOH	Oxidation potential = 0.8 V (vs. Ag/AgCl); Current density = 56.39 mA/cm <sup>2</sup>	-	-	-	-	[60]
NF	Ag	0.1 M Methanol	0.1 M NaOH	Oxidation potential = 0.440 V (vs. Ag/AgCl)	-	-	-	The current density of the N-AgNPs/NF electrode reached a steady state until 5000 s.	[6]
NF	AgPd	1.5 M Methanol	1.0 M NaOH	Onset potential = -0.36 V (vs. Ag/AgCl); Oxidation potential = -0.12 V (vs. Ag/AgCl); Current density = 7.673 mA/cm <sup>2</sup>	Mass activity = 1.887 A/mg <sub>Pd</sub>	ECSA/surface area = 24.5 m <sup>2</sup> /g	-	The decrease in forward current has only a ~9% after 50 cycles	[59]
NF	Pt/CoSe/ NiSe	1.0 M Methanol	1.0 M KOH	-	$I_f/I_b$ = 5.02; Mass activity = 1437.1 mA	ECSA/surface area = 85 m <sup>2</sup> /g <sub>Pt</sub> ; $R_{ct}$ = 9.6 $\Omega$	-	The decay corresponding to the ratio of current at 3600 s to initial current ( $I_{3600}/I_{initial}$ ) is approximately 0.72	[57]
NF	Pt-CoNi-LDH	0.5 M Methanol	1.0 M NaOH	-	$I_f/I_b$ = 2.06	ECSA/surface area = 131.86 m <sup>2</sup> /g	-	High current than Pt/C/NF for 6000 s at 0.10 V	[30]

Table 1. Cont.

Foam	Catalyst	Fuel Concentration (M)	Medium	Onset Potential, Oxidation Potential, Current Density	$I_f/I_b$ , Mass Activity	ECSA/Surface Area, Charge Transfer Resistance ( $R_{ct}$ ), Electron Transfer	Activation Energy, Power Density	Stability, Durability and Other Information	Ref.
NF	NiO	0.3 M Methanol	1.0 M KOH	Oxidation potential = 0.6 V (Hg/HgO); Current density = 161.5 mA/cm <sup>2</sup>	-	$R_{ct}$ = 0.4 $\Omega$	-	The electrodes current reveal no obvious decay within 3600 s and the current retention is >92% after 500 cycles	[72]
NF	NiO	0.4 M Methanol	1.0 M NaOH	Onset potential = 0.2–0.4 V; Oxidation potential = 0.6 V; Current density = 257 mA/cm <sup>2</sup>	-	ECSA/surface area = 4.56 m <sup>2</sup> /g	-	The CAs reached stability in a few seconds and the electrooxidation current density increases with the increase of applied potential.	[48]
NF	NiO	1.0 M Methanol	1.0 M KOH	Onset potential = 0.2–0.4 V (vs. Hg/HgO); Oxidation potential = 0.54 V (vs. Hg/HgO); Current density = 479 mA/cm <sup>2</sup>	$I_f/I_b > 1$	ECSA/surface area = 11.9 m <sup>2</sup> /g	-	After 3 h of CA testing, the shape was clearly maintained without any change and stable for 60 min.	[20]
NF	NiO nanosheet @ nanowires	0.5 M Methanol	1.0 M KOH	Oxidation potential = 1.62 V (vs. RHE); Current density = 89 mA/cm <sup>2</sup>	-	$R_{ct}$ = 1.1 $\Omega$	-	All electrodes show no decay in 8000 s and retains 81% of the anodic current density at 1.62 V after 1000 cycles	[73]
NF	NiO-CoO	0.5 M Methanol	1.0 M KOH	Onset potential = 0.35 V (vs. Hg/HgO); Current density = 175 $\mu$ A/cm <sup>2</sup> at 0.6 V	-	-	-	The current density of the NiO-CoO/NF electrode gradually decreased from 110 to 85 A/cm <sup>2</sup> within the initial 2.5 h	[75]

Table 1. Cont.

Foam	Catalyst	Fuel Concentration (M)	Medium	Onset Potential, Oxidation Potential, Current Density	$I_f/I_b$ , Mass Activity	ECSA/Surface Area, Charge Transfer Resistance ( $R_{ct}$ ), Electron Transfer	Activation Energy, Power Density	Stability, Durability and Other Information	Ref.
NF	C/Co <sub>3</sub> O <sub>4</sub>	0.5 M Methanol	0.5 M KOH	Onset potential = 0.39 V (vs. Hg/HgO)	-	ECSA/surface area = 85.7 m <sup>2</sup> /g; $R_{ct}$ = 5.21 $\Omega$	-	MOR at 0.6 V (vs. Hg/HgO) exhibits about 80% retention of the original value after 600 scans.	[68]
NF	Co(OH) <sub>2</sub>	0.5 M Methanol	0.5 M KOH	Onset potential = 0.27 V (vs. SCE)	Mass activity = 150 A/g	$R_{ct}$ = 1.4 $\Omega$	-	CA test showed the 84% retention based on the initial. CV curves of Co(OH) <sub>2</sub> catalyst are quite stable and the current density exhibits 82% retention after 500 cycles.	[69]
NF	Co <sub>3</sub> O <sub>4</sub>	0.5 M Methanol	1.0 M KOH	Onset potential = 0.32–0.34 V (vs. Hg/HgO)	Mass activity = 28–36.2 A/g at 0.6 V (vs. Hg/HgO)	ECSA/surface area = 53–100 m <sup>2</sup> /g	-	The current retentions of nanograss Co <sub>3</sub> O <sub>4</sub> , microsphere- Co <sub>3</sub> O <sub>4</sub> and microflower- Co <sub>3</sub> O <sub>4</sub> materials in methanol solution after 1000 cycles at a potential of 0.6 V are found to be 66, 96 and 32%, respectively.	[5]
NF	NiCo <sub>2</sub> O <sub>4</sub>	0.5 M Methanol	1.0 M KOH	-	Mass Activity = 40.9 A/g	ECSA/surface area = 146.5 m <sup>2</sup> /g	-	The current density performs 89% retention after 500 cycles. The current density can be returned to 97% of the original value by replacing the new solution.	[65]

Table 1. Cont.

Foam	Catalyst	Fuel Concentration (M)	Medium	Onset Potential, Oxidation Potential, Current Density	$I_f/I_b$ , Mass Activity	ECSA/Surface Area, Charge Transfer Resistance ( $R_{ct}$ ), Electron Transfer	Activation Energy, Power Density	Stability, Durability and Other Information	Ref.
NF	NiCo <sub>2</sub> O <sub>4</sub>	0.5 M Methanol	1.0 M KOH	Onset potential = 0.16 V (vs. SCE); Current density = 134 mA/cm <sup>2</sup>	-	$R_{ct} = 0.86 \Omega \text{ cm}^2$	-	CA tests are performed at 0.6 V for 1000 s showed stability 88%.	[77]
NF	ZnCo <sub>2</sub> O <sub>4</sub>	0.5 M Methanol	1.0 M KOH	Onset potential = 0.50 V (vs. Ag/AgCl)	Mass activity = 110 A/g	ECSA/surface area = 66 m <sup>2</sup> /g	-	65% of the current density retention observed after 1000 CV cycles.	[62]
NF	MgCo <sub>2</sub> O <sub>4</sub>	0.5 M Methanol	1.0 M KOH	Onset potential = 0.32 V (vs. Ag/AgCl)	Mass activity = 98 A/g	-	-	The current density retained was 73% after 1000 cycles. But the current density can be returned to 94% of the original value by replacing with new solution	[62]
GF	Pt	1.0 M Methanol	0.5 M H <sub>2</sub> SO <sub>4</sub>	Onset potential = 0–0.1 V (vs. Ag/AgCl); Oxidation potential = 0.6–0.8 V (vs. Ag/AgCl)	$I_f/I_b = 1.3$ ; Mass activity = 113.8 mA/mg <sub>Pt</sub>	ECSA/surface area = 67.5 cm <sup>2</sup> /g	-	-	[22]
GF	Pd	1.0 M Methanol	1.0 M KOH	Onset potential = –0.64 V (vs. SCE)	Mass activity = 0.835 A/mg <sub>Pd</sub>	ECSA/surface area = 59 m <sup>2</sup> /g	-	Pd/GF well reserved the much higher current density after 10,000 s for the MOR reactions as compared to the Pd/C	[12]

Table 1. Cont.

Foam	Catalyst	Fuel Concentration (M)	Medium	Onset Potential, Oxidation Potential, Current Density	$I_f/I_b$ , Mass Activity	ECSA/Surface Area, Charge Transfer Resistance ( $R_{ct}$ ), Electron Transfer	Activation Energy, Power Density	Stability, Durability and Other Information	Ref.
GF	PtRu	1.0 M Methanol	0.5 M H <sub>2</sub> SO <sub>4</sub>	Oxidation potential = 0.8–1.0 V (vs. SCE); Current density = 109.3 mA/cm <sup>2</sup>	$I_f/I_b = 1.14$	ECSA/surface area = 186.2 m <sup>2</sup> /g	-	The current density of PtRu/C, PtRu/Graphene, PtRu/GF were reduced by 78.8%, 54.6%, and 0.7% of their initial current density for MOR after 900 cycles, respectively	[35]
GA-NF	Pd	1.0 M Methanol	1.0 M KOH	Onset potential = 0.18 V (vs. SCE)	$I_f/I_b = 3.11$ ; Mass activity = 798.8 A/g	-	-	-	[89]
G-NF	Pt	1.0 M Methanol	0.5 M KOH	Onset potential = 0.42–0.45 V; Oxidation potential = 0.04 V; Current density = 139.0 mA/cm <sup>2</sup>	$I_f/I_b = 18.2$	ECSA/surface area = 150.3 m <sup>2</sup> /g; $R_{ct} = 4.9 \Omega$	-	The current density of Pt/G-Gel/NF-4 became stable to 3600 s	[45]
GO-NF	Pt-polyoxo-metalate	1.0 M Methanol	0.1 M KOH	Current density = 61.9 mA/cm <sup>2</sup>	$I_f/I_b = 5.1$ ; Mass activity = 250.6 mA/mg	ECSA/surface area = 69.3 m <sup>2</sup> /g	-	Showed the highest mass activity until 7200 s.	[76]
rGO-NF	Ni	10 $\mu$ M to 4.5 mM Methanol	0.1 M NaOH	Oxidation potential = 1.65 V (vs. RHE); Current density = 4.81 mA/cm <sup>2</sup>	-	$R_{ct} = 95 \Omega$	-	-	[78]
G-NF	NiCo <sub>2</sub> O <sub>4</sub>	0.5 M Methanol	1.0 M KOH	Onset potential = 0.4 V (vs. Hg/HgO)	Mass activity = 93.3 A/g at 0.65 V (vs. Hg/HgO)	$R_{ct} = 1.52 \Omega$	-	The current density has 93.4% retention of the first cycle after 500 cycles.	[77]

Table 1. Cont.

Foam	Catalyst	Fuel Concentration (M)	Medium	Onset Potential, Oxidation Potential, Current Density	$I_f/I_b$ , Mass Activity	ECSA/Surface Area, Charge Transfer Resistance ( $R_{ct}$ ), Electron Transfer	Activation Energy, Power Density	Stability, Durability and Other Information	Ref.
NF	Pd	0.5 M Ethanol	1.0 M KOH	-	Mass activity = 635 A/g	-	-	-	[54]
NF	Pd	0.25 M Ethanol	0.1 M NaOH	Onset potential = 0.5 V (vs. RHE); Oxidation potential = 1.15 V (vs. RHE)	-	$R_{ct} = 0.175 \Omega$	Activation energy = 17 kJ/mol	-	[37]
NF	Pd	1.0 M Ethanol	1.0 M KOH	Onset potential = 0.27 V (vs. RHE); Current density = 0.2 A	-	ECSA/surface area = 63 m <sup>2</sup> /g	Power density = 164 mW/cm <sup>2</sup>	-	[53]
NF	Pd	0.25 M Ethanol	0.1 M NaOH	Oxidation potential = 1.4–1.5 V (vs. RHE)	-	ECSA/surface area = 13,190 cm <sup>2</sup> /g	Activation energy = 12 kJ/mol	-	[40]
NF	Pd	0.25 M Ethanol	0.1 M NaOH	Onset potential = 0.45 V (vs. RHE); Oxidation potential = 0.8 V (vs. RHE)	-	-	Activation energy = 73.8 kJ/mol	-	[37]
NF	Pt	0.5 M Ethanol	0.1 M NaOH	Oxidation potential = 1.0–1.3 V (vs. RHE)	-	-	-	-	[84]
NF	PtSn	0.5 M Ethanol	0.1 M NaOH	Oxidation potential = 1.5–2.0 V (vs. RHE)	Mass activity = 1.75 A/g	-	-	-	[85]
NF	Pd-Ni(OH) <sub>2</sub>	1.0 M Ethanol	1.0 M NaOH	Oxidation potential = 0.8 V (vs. RHE)	Mass activity = 1295 mA/mg	ECSA/surface area = 24.61 m <sup>2</sup> /g <sub>Pd</sub> ; $R_{ct} = 0.49 \Omega$	-	Demonstrated excellent cycling stability and retained 89.6% of its initial activity after 2000 CV cycles	[83]
NF	Au	1.0 M Ethanol	0.5 M NaOH	Onset potential = 0.63 V (vs. Ag/AgCl); Oxidation potential = 0.15 V (vs. Ag/AgCl)	-	$R_{ct} = 62.5 \Omega$	-	~18.8% decline in the current density is observed after 900 s.	[86]

Table 1. Cont.

Foam	Catalyst	Fuel Concentration (M)	Medium	Onset Potential, Oxidation Potential, Current Density	$I_f/I_b$ , Mass Activity	ECSA/Surface Area, Charge Transfer Resistance ( $R_{ct}$ ), Electron Transfer	Activation Energy, Power Density	Stability, Durability and Other Information	Ref.
NF	NiO	0.05 M Ethanol	1.0 M NaOH	Onset potential = 0.2–0.4 V; Current density = 87 mA/cm <sup>2</sup> at 0.6 V	-	ECSA/surface area = 4.59 cm <sup>2</sup> /g	-	-	[48]
NF	NiO	2 M Ethanol	1.0 M KOH	Onset potential = 0.2–0.4 V (vs. Hg/HgO); Current density = 543 mA/cm <sup>2</sup>	-	ECSA/surface area = 11.9 m <sup>2</sup> /g	-	The current density is stable for 60 min.	[20]
GF	Pd	1.0 M Ethanol	1.0 M KOH	Onset potential = −0.5 V (vs. Hg/HgO)	-	-	-	The peak current density exhibits negligible change after the 100th cycle	[89]
GF	PdCo	1.0 M Ethanol	1.0 M KOH	Oxidation potential = −0.2 V (vs. SCE)	-	-	-	The EOR is relatively stable during the 2500 s testing time	[87]
GF	PdNi	0.1 M Ethanol	0.1 M KOH	Onset potential = −0.58 V (vs. MMO)	Mass activity = 0.372 A/mg	ECSA/surface area = 24.5 m <sup>2</sup> /g	-	The Pd <sub>1</sub> Ni <sub>2</sub> /CF yields a higher current than the Pd/CF within 10,000 s.	[81]
GF	PtRu	1.0 M Ethanol	0.5 M H <sub>2</sub> SO <sub>4</sub>	Oxidation potential = 0.8–1.0 V (vs. SCE); Current density = 78.6 mA/cm <sup>2</sup>	$I_f/I_b = 1$	ECSA/surface area = 186.2 m <sup>2</sup> /g	-	The current density of PtRu/C, PtRu/Graphene, PtRu/GF were decreased by 98.1%, 92.3%, and 67.5% of their initial current density for EOR after 900 cycles.	[35]
GF	PtCo-Pt skin	0.5 M Ethanol	0.1 M KOH	Onset potential = −0.55 V (vs. Ag/AgCl)	$I_f/I_b = 1.51$ ; Mass activity = 5.11 A/mg <sub>Pt</sub>	-	-	-	[88]

Table 1. Cont.

Foam	Catalyst	Fuel Concentration (M)	Medium	Onset Potential, Oxidation Potential, Current Density	$I_f/I_b$ , Mass Activity	ECSA/Surface Area, Charge Transfer Resistance ( $R_{ct}$ ), Electron Transfer	Activation Energy, Power Density	Stability, Durability and Other Information	Ref.
GA-NF	Pd	1.0 M Ethanol	1.0 M KOH	Onset potential = 0.564 V (vs. SCE)	$I_f/I_b = 2.72$ ; Mass activity = 874 A/g	-	-	The 7.65 wt% Pd/GA/NF electrode achieved better overall performance and stability in EOR compared to MOR.	[90]
Graphite coated NF	Pd	1.0 M Ethanol	1.0 M KOH	Onset potential = -601 mV (vs. Hg/HgO); Oxidation potential = -193 mV (vs. Hg/HgO); Current density = 39.97 mA/cm <sup>2</sup>	-	ECSA/surface area = 58.84 m <sup>2</sup> /g	-	The peaking current density of the as-prepared catalysts was about 2.64 times as high as that of commercial Pd/C to EOR.	[33]
rGO-NF	Pd	1.0 M Ethanol	0.5 M NaOH	Oxidation potential = 0.02 V (vs. Ag/AgCl); Current density = ~130 mA/cm <sup>2</sup>	$I_f/I_b = 0.87$	-	-	Current density on the Pd/ERGO was significantly slower to decay for 3200 s.	[93]
Carbon-NF	Pd	1.0 M Ethanol	1.0 M KOH	Onset potential = 0.3 V (vs. RHE); Current density = 0.16 A/cm <sup>2</sup>	-	ECSA/surface area = 121.8 m <sup>2</sup> /g	Power density = 202 mW/cm <sup>2</sup>	Stable in 16 h discharge at 100 mA/cm <sup>2</sup>	[49]
GA-NF	PdPt	4.0 M Ethanol	5.0 M KOH	-	-	-	Power density = 3.6 mW/cm <sup>2</sup>	-	[91]
GA-NF	PdPt	1.0 M Ethanol	1.0 M KOH	Oxidation potential = 0.245 V (vs. SCE)	$I_f/I_b = 1.24$ ; Mass activity = 3408.7 A/g	-	-	The Pd <sub>1</sub> Pt <sub>1.03</sub> /GA-NF electrode exhibits high activity and stability in EOR under a long operation (1000 cycles)	[92]

Table 1. Cont.

Foam	Catalyst	Fuel Concentration (M)	Medium	Onset Potential, Oxidation Potential, Current Density	$I_f/I_b$ , Mass Activity	ECSA/Surface Area, Charge Transfer Resistance ( $R_{ct}$ ), Electron Transfer	Activation Energy, Power Density	Stability, Durability and Other Information	Ref.
NF	Au	0.05–0.2 M NaBH <sub>4</sub>	2.0 M NaOH	Oxidation potential = −0.7 V (vs. Ag/AgCl); Current density = 827 mA/cm <sup>2</sup>	-	-	-	After 1200 s test, the oxidation current densities of 170 mA/cm <sup>2</sup> , 35 mA/cm <sup>2</sup> and 4 mA/cm <sup>2</sup> can be obtained at −0.4 V, −0.6 V and −0.8 V, respectively	[50]
NF	NiCo	0.1 M NaBH <sub>4</sub>	1.0 M NaOH	Onset potential = −1.0 V (vs. Ag/AgCl)	-	-	-	The current density reached steady state at all applied potentials after a rapid decrease	[95]
NF	CuNiPd	0.3 M NaBH <sub>4</sub>	2.0 M NaOH	Current density = 710 mA/cm <sup>2</sup> at 0 V	-	Electron transfer = 4.9	Activation energy = 18.42 kJ/mol	The current density is maintain after change several potential.	[31]
NF	PtCo-Co <sub>3</sub> O <sub>4</sub>	0.2 M NaBH <sub>4</sub>	2.0 M NaOH	Current density = 850 mA/cm <sup>2</sup> at −0.4 V	-	-	-	the current densities become stable after only dozens of seconds when the applied potentials are fixed at −0.6, −0.8, and −1.0 V	[51]
NF	CoSn <sub>0.33</sub> -B	0.2 M KBH <sub>4</sub>	1.0 M KOH	-	-	-	Power density = 158 mW/cm <sup>2</sup>	Specific capacity or fuel conversion efficiency decrease with the catalytic activity increases.	[94]
rGOF	Au	0.4 M NaBH <sub>4</sub>	2.0 M NaOH	Current density = 661 mA/cm <sup>2</sup>	-	Electron transfer = 7.2	Power density = 50 mW/cm <sup>2</sup>	Open-circuit voltage (OCV) of 1.60 V	[98]
rGOF	CoAu	0.3 M NaBH <sub>4</sub>	2.0 M NaOH	Current density = 1.35 A/cm <sup>2</sup> at 0 V	-	ECSA/surface area = 390 m <sup>2</sup> /g; Electron transfer = 6.9	Power density = 80.5 mW/cm <sup>2</sup> at 85 mA/cm <sup>2</sup>	55.4% utilization efficiency of NaBH <sub>4</sub>	[99]

Table 1. Cont.

Foam	Catalyst	Fuel Concentration (M)	Medium	Onset Potential, Oxidation Potential, Current Density	$I_f/I_b$ , Mass Activity	ECSA/Surface Area, Charge Transfer Resistance ( $R_{ct}$ ), Electron Transfer	Activation Energy, Power Density	Stability, Durability and Other Information	Ref.
rGOF	CoNi	0.5 M NaBH <sub>4</sub>	4.0 M NaOH	Current density = 1.54 A/cm <sup>2</sup>	-	$R_{ct}$ = 0.286 $\Omega$ cm <sup>2</sup> ; Electron transfer = 6.7	Activation energy = 8.29 kJ/mol; Power density = 140 mW/cm <sup>2</sup>	-	[100]
NF	NiCo	0.33 M Urea	5.0 M KOH	-	-	-	Power density = 17.4 mW/cm <sup>2</sup> and 31.5 mW/cm <sup>2</sup> at 20 °C and 70 °C, respectively.	Open circuit voltage of 0.83 V	[101]
NF	NiRh	0.05 M Urea	1.0 M KOH	Onset potential = 0.33 V; Current density = 131.9 mA/cm <sup>2</sup>	-	-	-	The retention current is 17.4% in comparison between 50 s and 1800 s	[106]
NF	NiO	0.1 M Urea	1.0 M NaOH	Onset potential = 0.2–0.4 V; Current density = 155 mA/cm <sup>2</sup> at 0.6 V	-	ECSA/surface area = 4.59 cm <sup>2</sup> /g	-	The potential of 0.30 V is close to the onset oxidation potential and the stable current density is only around 2 mA/cm <sup>2</sup> at this potential.	[48]
NF	NiO	0.33 M Urea	1.0 M KOH	Onset potential = 0.35 V (vs. Hg/HgO); Current density = 800 mA/cm <sup>2</sup> at 0.7 V	-	-	-	Did not show any morphology change after being used for urea electro-oxidation for 12 h.	[108]
NF	Ni(OH) <sub>2</sub>	0.6 M Urea	5.0 M KOH	Onset potential = 0.21 V (vs. Ag/AgCl); Current density = 559 mA/cm <sup>2</sup> at 0.56 V (vs. Ag/AgCl)	-	-	Power density = 19.7 mW/cm <sup>2</sup> and 28.8 mW/cm <sup>2</sup> at 20 °C and 50 °C, respectively.	Open circuit voltage of 0.86 V	[102]

Table 1. Cont.

Foam	Catalyst	Fuel Concentration (M)	Medium	Onset Potential, Oxidation Potential, Current Density	$I_f/I_b$ , Mass Activity	ECSA/Surface Area, Charge Transfer Resistance ( $R_{ct}$ ), Electron Transfer	Activation Energy, Power Density	Stability, Durability and Other Information	Ref.
NF	Ni(OH) <sub>2</sub>	0.33 M Urea	2.0 M KOH	Onset potential = 0.35 V (vs. Hg/HgO)	-	$R_{ct}$ = 0.4 $\Omega$	-	Negligible change in potential over the operation period of 5 h.	[107]
NF	Se-Ni(OH) <sub>2</sub> shelled-NiSe nanowire	0.33 M Urea	1.0 M KOH	Current density = 100 mA/cm <sup>2</sup> at 0.366 V (vs. SCE)	-	$R_{ct}$ = 6 $\Omega$	-	The potential remains constant for the rest of 500 s	[105]
NF	NiCo <sub>2</sub> S <sub>4</sub> nanowire	0.33 M Urea	5.0 M KOH	Onset potential = 0.18 V (vs. Ag/AgCl); Current density = 720 mA/cm <sup>2</sup>	-	$R_{ct}$ = 0.12 $\Omega$	-	The current densities at different potentials nearly stable after 7200 s	[104]
NF	NiCoO <sub>4</sub> nanowire	0.33 M Urea	5.0 M KOH	Onset potential = 0.19 V (vs. Ag/AgCl); Current density = 570 mA/cm <sup>2</sup> at 0.6 V	-	-	-	The current density remained nearly constant without any reduction after 1800 s	[108]
NF	-	1.0 M Glucose	3.0 M KOH	Current density = 0.03 A/cm <sup>2</sup>	-	Mediator = methyl viologen	Power density = 0.62 mW/cm <sup>2</sup> at current density 5.03 mA/cm <sup>2</sup>	-	[110]
NF	-	1.0 M Glucose	3.0 M KOH	-	-	Mediator = methyl viologen	Power density = 5.20 W/m <sup>2</sup> at 15 mM methyl viologen	Specific capacity = 153.58 mAh/g	[111]
NF	-	1.0 M Glucose	3.0 M KOH	-	-	$R_{ct}$ = 0.4522 $\Omega$ ; Mediator = 4-naphthoquinone (NQ)	Power density = 16.10 W/cm <sup>2</sup> at current density 48.09 A/m <sup>2</sup>	Open circuit voltage of 0.76 V	[113]

Table 1. Cont.

Foam	Catalyst	Fuel Concentration (M)	Medium	Onset Potential, Oxidation Potential, Current Density	$I_f/I_b$ , Mass Activity	ECSA/Surface Area, Charge Transfer Resistance ( $R_{ct}$ ), Electron Transfer	Activation Energy, Power Density	Stability, Durability and Other Information	Ref.
NF	Au	0.5 M Glucose	6.0 M KOH	-	-	-	Power density = 26.6 W/cm <sup>2</sup> at current density 89 mA/cm <sup>2</sup>	-	[114]
NF	Ag	0.5 M Glucose	0.5 M KOH	-	-	-	Power density = 2.03 mW/cm <sup>2</sup> at 80 °C	-	[112]
GA-NF	PdPt	0.5 M Glucose	3.0 M KOH	-	-	-	Power density = 1.25 mW/cm <sup>2</sup>	Open circuit voltage (OCV) of the cell at 1.1 V	[115]
rGO-NF	NiO	1.0 M Glucose	3.0 M KOH	-	-	$R_{ct} = 0.1576 \Omega$	Power density = 13.48 W/m <sup>2</sup>	OCV = 0.792 V	[116]
rGO-NF	-	10 $\mu$ M–4.5 mM Glucose	0.1 M NaOH	Onset Potential = 1.4 V	-	-	-	-	[78]
G-NF	Pd-ZnO	0.5 M Glucose	1.0 M KOH	Oxidation potential = 0.742 V; Current density = 222.2 mA/cm <sup>2</sup>	$I_f/I_b = 1.96$	-	-	-	[117]
Cu/CuO <sub>2</sub> Foam	Metal-Doped (M = Ni, Co, Fe)	2.0 mM Glucose	0.1 M KOH	Oxidation potential = 0.5 V (vs. SCE); Current density = 30 mA/cm <sup>2</sup>	-	-	-	-	[119]
NF	Ni	0.25–2 M H <sub>2</sub> O <sub>2</sub>	4.0 M KOH	Onset potential = −0.2 V; Current density = 822 mA/cm <sup>2</sup> at 0.2 V	-	-	Activation energy = 21.2 kJ/mol; Power density = 19.4 mW/cm <sup>2</sup>	Oxidation currents were nearly constant at each potential during the test period 3000 s	[125]
NF	Ni	1 M H <sub>2</sub> O <sub>2</sub>	4.0 M KOH	-	-	-	Power density = 22.8 mW/cm <sup>2</sup>	-	[121]

Table 1. Cont.

Foam	Catalyst	Fuel Concentration (M)	Medium	Onset Potential, Oxidation Potential, Current Density	$I_f/I_b$ , Mass Activity	ECSA/Surface Area, Charge Transfer Resistance ( $R_{ct}$ ), Electron Transfer	Activation Energy, Power Density	Stability, Durability and Other Information	Ref.
NF	Ni	1 M H <sub>2</sub> O <sub>2</sub>	4.0 M KOH	-	-	-	Power density = 36 mW/cm <sup>2</sup> at 20 °C	OCP of 1.09 V	[122]
NF	NiCoO <sub>4</sub>	0.4 M H <sub>2</sub> O <sub>2</sub>	3.0 M KOH	Current density = 330 mA/cm <sup>2</sup> at 0.6 V	-	-	-	The curves remained smooth without any fluctuation during the 1200 s test period at low reduction potential	[126]
NF	Pd	0.5 M Glycerol	1.0 M KOH	-	Mass activity = 1470 A/g	-	-	-	[54]
GF	Pd	1.0 M Glycerol	1.0 M KOH	Onset potential = -0.45 V (vs. SCE)	Mass activity = 2.718 A/mg Pd; ESCA/ surface area = 59 m <sup>2</sup> /g	-	-	Pd/GF well reserved the much higher current density after 10,000 s for all the EGOR and GOR reactions as compared to the Pd/C	[12]
GF	Pd	1.0 M Ethylene Glycol	1.0 M KOH	Onset potential = -0.53 V (vs. SCE)	Mass activity = 4.056 A/g Pd; ESCA/ surface area = 59 m <sup>2</sup> /g	-	-	-	[12]
NF	Pd	0.5 M Ethylene Glycol	1.0 M KOH	-	Mass activity = 2100 A/g	-	-	-	[54]
NF	NiZn	0.1 M N <sub>2</sub> H <sub>4</sub>	1.0 M NaOH	Onset potential = -0.08 V (vs. RHE); Current density = 370 mA/cm <sup>2</sup> at 0.3 V	-	-	-	The catalytic performance of NiZn catalyst maintains 88.7%; however, the NF and Ni film only remain 58.1% and 59.1% of the initial activity after 5000 s, respectively.	[130]
NF	Ni(OH) <sub>2</sub> / NiOOH	0.03 M Ammonia	10 mM Na <sub>2</sub> SO <sub>4</sub>	Onset potential = 0.6 V (vs. Hg/HgO at pH 11)	-	-	-	-	[128]

Table 1. Cont.

Foam	Catalyst	Fuel Concentration (M)	Medium	Onset Potential, Oxidation Potential, Current Density	$I_f/I_b$ , Mass Activity	ECSA/Surface Area, Charge Transfer Resistance ( $R_{ct}$ ), Electron Transfer	Activation Energy, Power Density	Stability, Durability and Other Information	Ref.
NF	Ni phosphide nanowire	Not mention	1.0 M NaOH	Onset potential = $-0.08$ V (vs. RHE); Current density = $580$ mA/cm <sup>2</sup> at $0.3$ V	-	-	-	After 10000 s of constant-potential measurement, the Ni <sub>x</sub> P/NF catalyst still retained 80.5% of its initial activity	[129]
Foam	Catalyst	Fuel Concentration (M)	Medium	Onset Potential, Reduction Potential, Current Density	$I_f/I_b$ , Mass Activity	ECSA/Surface Area, Charge Transfer Resistance ( $R_{ct}$ ), Electron Transfer	Activation Energy, Power Density	Stability, Durability, and Other Information	Ref.
rGO-NF	Pd	0.5 M H <sub>2</sub> O <sub>2</sub>	2.0 M NaOH	Current density = $450$ mA/cm <sup>2</sup> at $0.8$ V	-	ECSA/ surface area = $67.97$ m <sup>2</sup> /g	Activation energy = $8.202$ kJ/mol	All of the curves keep smooth and stable immediately after the start of the test for H <sub>2</sub> O <sub>2</sub> reduction	[120]
Carbon Sponge	PtCo	1.5 M H <sub>2</sub> O <sub>2</sub>	3.0 M KOH	Reduction potential = $-0.30$ to $-0.6$ V; Current density = $-1.38$ A/cm <sup>2</sup> .mg at $-0.5$ V (vs. Ag/AgCl)	-	-	-	Open circuit potentials (OCP) were $-0.16$ V	[52]
NF	Pd@SnO <sub>2</sub>	0.5 M H <sub>2</sub> O <sub>2</sub>	3.0 M NaOH	Current density = $320$ mA/cm <sup>2</sup> at $-0.54$ V	-	-	-	The catalyst changes barely during 800 potential cycles	[124]
NF	Co <sub>3</sub> O <sub>4</sub>	0.5 M H <sub>2</sub> O <sub>2</sub>	3.0 M KOH	Current density = $0.214$ A/cm <sup>2</sup> at $0.4$ V (vs. Ag/AgCl)	-	-	-	the open circuit potential (OCP) of the five samples are closed to $-0.15$ V	[127]

### 3.8. Selected Application of Foam in the Electrolyzers

Lin et al. [15] put forward the idea of adding phosphide to the binary alloy of NiFe and support on NF. The advantage of ruthenium (Ru) metal in increasing the reaction rate has led to super-low loading of Ru in NiFe-P/NF due to Ru's cost as a precious metal that provides highly catalytic activity in all pH media. The authors also claimed that the addition of Ru increases electron interaction and ultrasmall of overpotential. Zhao et al. [131] also use almost the same material without the presence of phosphate. Cheng et al. [132] also produced the Fe-Ni-based electrocatalyst for OER. To increase the capability of the water dissolution, robust stability, and ultra-high current density, the hybrid  $r\text{-FeOOH}$  and  $\alpha\text{-Ni(OH)}_2$  are produced on NF surfaces having amorphous and crystalline properties, respectively. Yang et al. has created ternary metal  $\text{Co}_{1-x}\text{V}_x\text{P}$  with nanoneedle structures supported on NF to increase the hydrogen evolution reaction (HER) [14]. The uniqueness of the structure made in this study has increased catalyst stability in the long run and has reduced overpotential and increased current density of 46 mV at 10 mA/cm<sup>2</sup> and 226 mV at 400 mA/cm<sup>2</sup>, respectively. In the theoretical study by Park et al., the use of  $\text{Co}_{1-x}\text{V}_x\text{P}$  catalyst reduced the activation energy during the dissociation of water. Nanosheets of  $\text{Co}_3\text{S}_4$  directly synthesize on the NF surface through electrodeposition and sulfurization and create a more active site and accessible surface reactant for HER [133]. The authors also studied the effect of time in the sulfurization process on the formation of Cobalt sulfide on the NF surface. The optimized catalyst has produced excellent durability without overpotential and in single-cell changes in 220 h and 720 min, respectively. Metal oxide also has the advantage of increasing the current density produced by Wang et al. [134]. Wang et al. [134] synthesized the  $\text{MoO}_2$  at surface NF, doping with phosphorus (P) and tungsten (W). Authors claim the addition of P and W's heteroatoms accelerated the charge transfer, facilitated the electron interaction, and tuned the electron environment.

## 4. Conclusions

The demand for energy consumption is on the rise. Therefore, a more consistent, active, and productive study of the high activity of the electro-oxidation reaction in DLFCs is essential to address the issues that have been mentioned in this paper. Common problems in electrocatalysts are low stability and durability, slow kinetics, catalyst poisoning, high catalyst loading, high cost of the catalytic materials, poisoning of the electrocatalysts, and formation of the intermediate products during the electrochemical reactions. One way to increase activity is by using appropriate support materials such as carbon black, carbon aerogels, carbon nanotubes, mesoporous carbon, graphene oxide, and graphene nanosheets. Support material should have characteristics such as large surface area, low surface poisoning, high porosity, multiple active sites for the reaction to occur, high activity, good conductivity, and long-term stability. Commonly used support materials face problems; namely, their corrosion resistance leads to particle detachment, Ostwald ripening, and agglomeration. The selection of Nickel foam and graphene foam is seen to reduce the problems faced by other support materials. The 3D network structure in the nickel foam and graphene foam has high conductivity, controllable electrochemical properties, excellent mechanical strength, high surface area, high porosity, and low cost, and are suitable for use as catalyst supports. Powdery catalysts are commonly used in DLFCs that require a binder's involvement to make the electrode slurry. The binder's presence decreases the electrochemical activity, as the binder reduces the ion and electron transport occurring in the electrode and at the electrode/electrolyte interface by blocking the catalyst active sites. Therefore, the use of the 3D structured materials NF and GF can improve the performance when a binder is not required in the electrode. Besides, NF and GF's use has significantly reduced CO's ability to be adsorbed on the surface catalyst while further enhancing the catalytic activity, stability, and durability of the electrochemical reaction in the fuel cell. The CO molecules on the catalyst surface are reduced by improving the particle distribution, thus increasing the number of catalytic active sites for the electrochemical reactions. Exploring various types of catalyst structures supported on NF and GF in future research,

such as nanofilm, should be carried out in DLFCs because the layered structure has unique features that can increase electrochemical active surface area, most of which have been applied in other fields.

**Author Contributions:** Writing—original draft preparation, N.A.K.; Data collection, N.A.K. and M.S.A.; funding acquisition, N.A.K. and H.Y. All authors have read and agreed to the published version of the manuscript.

**Funding:** The authors gratefully acknowledge financial support by the Ministry of Education under FRGS/1/2019/TK02/UKM/02/4. The authors also gratefully acknowledge financial support for this work funded by the Ministry of Science and Technology of Taiwan (grant number: MOST-108-2221-E-005-026) and also partially supported by the Ministry of Education, Taiwan, R.O.C. under the Higher Education Sprout Project and New Southbound Scheme in research collaboration.

**Conflicts of Interest:** The authors declare that they have no conflict of interest.

### Acronyms

AQ	Anthraquinone
BOR	Borohydride Electro-Oxidation Reaction
CO	Carbon Monoxide
CoNPs	Co nanoparticles
CVD	Chemical Vapor Deposition
DA	1,5-Dichloro-Anhraquinone
DAFC	Direct Ammonia Fuel Cells
DBFC	Direct Borohydride Fuel Cell
DEFC	Direct Ethanol Fuel Cell
DEGFC	Direct Ethylene Glycol Fuel Cell
DGFC	Direct Glycerol Fuel Cell
DGluFC	Direct Glucose Fuel Cell
DHFC	Direct Hydrazine Fuel Cell
DLFC	Direct Liquid Fuel Cell
DMFC	Direct Methanol Fuel Cell
DUPFC	Direct Hydrogen Peroxide Fuel Cell
ECSA	Electrochemical Surface Area
EOR	Ethanol Oxidation Reaction
GA	Graphene Aerogel
GDL	Gas Diffusion Layer
GF	Graphene Foam
GluOR	Glucose Electro-Oxidation Reaction
H <sub>2</sub> O <sub>2</sub> OR	Hydrogen Peroxide Electro-Oxidation
H <sub>2</sub> O <sub>2</sub> RR	Hydrogen Peroxide Electro-Reduction Reaction
i <sub>f</sub> /i <sub>b</sub>	Forward Scan/Backward Scan
ITO	Indium Tin Oxide
LDH	Layered Double Hydroxides
MB	Methylene Blue
MEA	Membrane Electrolyte Assembly
MOR	Methanol Electro-Oxidation Reaction
MV	Methyl Viologen
NF	Nickel Foam
NQ	2-Hydroxy-1,4-Naphthoquinone
NR	Neutral Red
Pd	Palladium
PEMFC	Polymer Electrolyte Membrane Fuel Cells
Pt	Platinum
rGO	Reduced Graphene Oxide
SSFF	Stainless Steel Fiber Felt
UER	Urea Electro-Oxidation Reaction
ZIF-67	Zeolitic Imidazolate Framework-67

## References

1. Chen, X.; Ge, F.; Lai, N. Cobalt-Based coordination polymer as high activity electrocatalyst for oxygen reduction reaction: Catalysis by novel active site  $\text{CoO}_4\text{N}_2$ . *Int. J. Energy Res.* **2020**, *44*, 2164–2172. [[CrossRef](#)]
2. Deokate, R.J.; Mujawar, S.H.; Chavan, H.S.; Mali, S.S.; Hong, C.K.; Im, H.; Inamdar, A.I. Chalcogenide nanocomposite electrodes grown by chemical etching of Ni-foam as electrocatalyst for efficient oxygen evolution reaction. *Int. J. Energy Res.* **2020**, *44*, 1233–1243. [[CrossRef](#)]
3. Karim, N.; Rubinsin, N.; Burukan, M.; Kamarudin, S. Sustainable route of synthesis platinum nanoparticles using orange peel extract. *Int. J. Green Energy* **2019**, *16*, 1518–1526. [[CrossRef](#)]
4. Hanapi, I.; Kamarudin, S.; Zainoodin, A.; Hasran, U. Membrane-Less micro fuel cell system design and performance: An overview. *Int. J. Energy Res.* **2019**, *43*, 8956–8972. [[CrossRef](#)]
5. Rajeshkhanna, G.; Rao, G.R. Micro and nano-architectures of  $\text{Co}_3\text{O}_4$  on Ni foam for electro-oxidation of methanol. *Int. J. Hydrog. Energy* **2018**, *43*, 4706–4715. [[CrossRef](#)]
6. Yu, Y.; Cheng, Y.; Guo, M.; Li, C.; Hu, J. Ag nanoparticles supported on nickel foam: A flexible 3D electrode for methanol electrocatalytic oxidation. *RSC Adv.* **2017**, *7*, 39539–39545. [[CrossRef](#)]
7. Ince, A.C.; Karaoglan, M.U.; Glösen, A.; Colpan, C.O.; Müller, M.; Stolten, D. Semiempirical thermodynamic modeling of a direct methanol fuel cell system. *Int. J. Energy Res.* **2019**, *43*, 3601–3615. [[CrossRef](#)]
8. Ong, B.; Kamarudin, S.; Basri, S. Direct liquid fuel cells: A review. *Int. J. Hydrog. Energy* **2017**, *42*, 10142–10157. [[CrossRef](#)]
9. Yu, X.; Manthiram, A. Scalable membraneless direct liquid fuel cells based on a catalyst-selective strategy. *Energy Environ. Mater.* **2018**, *1*, 13–19. [[CrossRef](#)]
10. Velisala, V.; Srinivasulu, G.N.; Reddy, B.S.; Rao, K.V.K. Review on challenges of direct liquid fuel cells for portable application. *World J. Eng.* **2015**, *12*, 591–606. [[CrossRef](#)]
11. Fadzillah, D.; Kamarudin, S.; Zainoodin, M.; Masdar, M. Critical challenges in the system development of direct alcohol fuel cells as portable power supplies: An overview. *Int. J. Hydrog. Energy* **2019**, *44*, 3031–3054. [[CrossRef](#)]
12. Cui, X.; Li, Y.; Zhao, M.; Xu, Y.; Chen, L.; Yang, S.; Wang, Y. Facile growth of ultra-small Pd nanoparticles on zeolite-templated mesocellular graphene foam for enhanced alcohol electrooxidation. *Nano Res.* **2019**, *12*, 351–356. [[CrossRef](#)]
13. Shakibi Nia, N.; Guillén-Villafuerte, O.; Griesser, C.; Manning, G.; Kunze-Liebhäuser, J.; Arévalo, C.; Pastor, E.; García, G.  $\text{W}_2\text{C}$ -Supported PtAuSn—A catalyst with the earliest ethanol oxidation onset potential and the highest ethanol conversion efficiency to  $\text{CO}_2$  known till date. *ACS Catal.* **2020**, *10*, 1113–1122. [[CrossRef](#)]
14. Yang, M.; Shang, C.; Li, F.; Liu, C.; Wang, Z.; Gu, S.; Liu, D.; Cao, L.; Zhang, J.; Lu, Z.; et al. Synergistic electronic and morphological modulation on ternary  $\text{Co}_{1-x}\text{V}_x\text{P}$  nanoneedle arrays for hydrogen evolution reaction with large current density. *Sci. China Mater.* **2020**. [[CrossRef](#)]
15. Lin, Y.; Zhang, M.; Zhao, L.; Wang, L.; Cao, D.; Gong, Y. Ru doped bimetallic phosphide derived from 2D metal organic framework as active and robust electrocatalyst for water splitting. *Appl. Surf. Sci.* **2021**, *536*, 147952. [[CrossRef](#)]
16. Gamea, O.E.; Ookawara, S.; Mori, S.; Ahmed, M. Performance enhancement of direct methanol fuel cell using multi-zone narrow flow fields. *Int. J. Energy Res.* **2019**, *43*, 8257–8274.
17. Shrivastava, N.K.; Thombre, S.B.; Chadge, R.B. Liquid feed passive direct methanol fuel cell: Challenges and recent advances. *Ionics* **2015**, *22*, 1–23. [[CrossRef](#)]
18. Ning, X.; Zhou, X.; Luo, J.; Ma, L.; Xu, X.; Zhan, L. Glycerol and formic acid electro-oxidation over Pt on S-Doped carbon nanotubes: Effect of carbon support and synthesis method on the metal-support interaction. *Electrochim. Acta* **2019**, *319*, 129–137. [[CrossRef](#)]
19. Yahya, N.; Kamarudin, S.; Karim, N.; Masdar, M.; Loh, K.; Lim, K. Durability and performance of direct glycerol fuel cell with palladium-aurum/vapor grown carbon nanofiber support. *Energy Convers. Manag.* **2019**, *188*, 120–130. [[CrossRef](#)]
20. Eisa, T.; Mohamed, H.O.; Choi, Y.-J.; Park, S.-G.; Ali, R.; Abdelkareem, M.A.; Oh, S.-E.; Chae, K.-J. Nickel nanorods over nickel foam as standalone anode for direct alkaline methanol and ethanol fuel cell. *Int. J. Hydrog. Energy* **2020**, *45*, 5948–5959. [[CrossRef](#)]
21. Chen, X.; Zhang, Z.; Shen, J.; Hu, Z. Micro direct methanol fuel cell: Functional components, supplies management, packaging technology and application. *Int. J. Energy Res.* **2016**, *41*, 613–627. [[CrossRef](#)]
22. Zhang, Y.; Shao, Z.; Shen, Q.; Li, M.; Xu, L.; Luo, Z. Aqueous preparation of platinum nanoflowers on three-dimensional graphene for efficient methanol oxidation. *Catalysts* **2018**, *8*, 519. [[CrossRef](#)]
23. Zhang, J.; Chen, J.; Jiang, Y.; Zhou, F.; Zhong, J.; Wang, G.; Kiani, M.; Wang, R. Facile synthesis of flower-like platinum nanostructures as an efficient electrocatalyst for methanol electro-oxidation. *J. Colloid Interface Sci.* **2016**, *479*, 64–70. [[CrossRef](#)]
24. Kamyabi, M.A.; Mohammadian, H.; Jadali, S.; Moharramnezhad, M. Hydrothermal syntheses of NiO-GO nanocomposite on 3D nickel foam as a support for Pt nanoparticles and its superior electrocatalytic activity towards methanol oxidation. *Electroanalysis* **2019**, *31*, 1484–1493. [[CrossRef](#)]
25. Zhang, Y.-L.; Li, J.-L.; Zhao, L.; Sui, X.-L.; Zhou, Q.-Y.; Gong, X.-F.; Cai, J.-J.; Gu, D.-M.; Wang, Z.-B. Nitrogen doped carbon coated Mo modified  $\text{TiO}_2$  nanowires (NC@MTNWs-FI) with functionalized interfacial as advanced PtRu catalyst support for methanol electrooxidation. *Electrochim. Acta* **2020**, *331*, 135410. [[CrossRef](#)]
26. Li, P.-W.; Li, Y.-H.; Ma, Y.-M.; Li, Q.-X. Various morphology of  $\text{WO}_3$  modified activated carbon supported Pd catalysts with enhanced formic acid electrooxidation. *J. Nanosci. Nanotechnol.* **2019**, *19*, 7777–7784. [[CrossRef](#)]

27. Li, J.-L.; Zhao, L.; Li, X.-F.; Hao, S.-E.; Wang, Z.-B. Carbon-Coated and interfacial-functionalized mixed-phase  $\text{Mo}_x\text{Ti}_{1-x}\text{O}_{2-\delta}$  nanotubes as highly active and durable PtRu catalyst support for methanol electrooxidation. *Chem. Asian J.* **2019**, *14*, 1549–1556. [[CrossRef](#)]
28. Pham, H.Q.; Huynh, T.T.; Mai, A.T.N.; Ngo, T.M.; Bach, L.G.; Ho, V.T.T. Wire-Like Pt on mesoporous  $\text{Ti}_0.7\text{W}_0.3\text{O}_2$  nanomaterial with compelling electro-activity for effective alcohol electro-oxidation. *Sci. Rep.* **2019**, *9*, 1–9. [[CrossRef](#)] [[PubMed](#)]
29. Cheng, C.-K.; Yeh, T.-K.; Tsai, M.-C.; Chou, H.-Y.; Wu, H.-C.; Hsieh, C.-K. The hybrid nanostructure of vertically aligned cobalt sulfide nanoneedles on three-dimensional graphene decorated nickel foam for high performance methanol oxidation. *Surf. Coat. Technol.* **2017**, *320*, 536–541. [[CrossRef](#)]
30. Zhang, F.; Wang, Z.; Xu, K.Q.; Xia, J.; Liu, Q.; Wang, Z. Highly dispersed ultrafine Pt nanoparticles on nickel-cobalt layered double hydroxide nanoarray for enhanced electrocatalytic methanol oxidation. *Int. J. Hydrog. Energy* **2018**, *43*, 16302–16310. [[CrossRef](#)]
31. Song, C.; Wang, G.; Li, B.; Miao, C.; Ma, K.; Zhu, K.; Cheng, K.; Ye, K.; Yan, J.; Cao, D.; et al. A novel electrode of ternary CuNiPd nanoneedles decorated Ni foam and its catalytic activity toward  $\text{NaBH}_4$  electrooxidation. *Electrochim. Acta* **2019**, *299*, 395–404. [[CrossRef](#)]
32. Tang, B.; Lv, Y.; Du, J.; Dai, Y.; Pan, S.; Xie, Y.; Zou, J.  $\text{MoS}_2$ -Coated  $\text{Ni}_3\text{S}_2$  nanorods with exposed {110} high-index facets as excellent CO-tolerant cocatalysts for Pt: Ultradurable catalytic activity for methanol oxidation. *ACS Sustain. Chem. Eng.* **2019**, *7*, 11101–11109. [[CrossRef](#)]
33. Jiang, Y.; Zhou, F.; Chen, J.; Zhang, J.; Li, A.; Zeng, Y.; Wang, G. Ultralow loading palladium nanocatalysts prepared by atomic layer deposition on three-dimensional graphite-coated nickel foam to enhance the ethanol electro-oxidation reaction. *RSC Adv.* **2016**, *6*, 13207–13216. [[CrossRef](#)]
34. Yi, F.; Gao, Y.; Li, H.; Yi, L.; Chen, D.; Lu, S. Nitrogen- and oxygen-codoped porous carbonaceous foam templated from high internal emulsion as PtRu catalyst support for direct methanol fuel cell. *Electrochim. Acta* **2016**, *211*, 768–776. [[CrossRef](#)]
35. Kung, C.-C.; Lin, P.-Y.; Xue, Y.; Akolkar, R.; Dai, L.; Yu, X.; Liu, C.-C. Three dimensional graphene foam supported platinum–ruthenium bimetallic nanocatalysts for direct methanol and direct ethanol fuel cell applications. *J. Power Sources* **2014**, *256*, 329–335. [[CrossRef](#)]
36. Li, J.; Luo, F.; Zhao, Q.; Xiao, L.; Yang, J.; Liu, W.; Xiao, D. Crystalline nickel boride nanoparticle agglomerates for enhanced electrocatalytic methanol oxidation. *Int. J. Hydrog. Energy* **2019**, *44*, 23074–23080. [[CrossRef](#)]
37. Mikolajczyk, T.; Turemko, M.; Pierozynski, B. Ethanol oxidation reaction at Pd-Modified nickel foam obtained by PVD method in alkaline solution. *J. Electroanal. Chem.* **2014**, *735*, 32–35. [[CrossRef](#)]
38. Zhang, C.; Lee, B.-J.; Li, H.; Samdani, J.; Kang, T.-H.; Yu, J.-S. Catalytic mechanism of graphene-nickel interface dipole layer for binder free electrochemical sensor applications. *Commun. Chem.* **2018**, *1*, 94. [[CrossRef](#)]
39. Sim, Y.; Kwak, J.; Kim, S.-Y.; Jo, Y.; Kim, S.; Kim, S.Y.; Kim, J.H.; Lee, C.-S.; Jo, J.H.; Kwon, S.-Y. Formation of 3D Graphene-Ni foam heterostructures with enhanced performance and durability for bipolar plates in a polymer electrolyte membrane fuel cell. *J. Mater. Chem. A* **2017**, *6*, 1504–1512. [[CrossRef](#)]
40. Pierozynski, B.; Mikolajczyk, T.; Turemko, M. On the temperature performance of ethanol oxidation reaction at palladium-activated nickel foam. *Electrocatalysis* **2015**, *6*, 173–178. [[CrossRef](#)]
41. Roy, A.; Jadhav, H.S.; Cho, M.; Gil Seo, J. Electrochemical deposition of self-supported bifunctional copper oxide electrocatalyst for methanol oxidation and oxygen evolution reaction. *J. Ind. Eng. Chem.* **2019**, *76*, 515–523. [[CrossRef](#)]
42. Cheng, Y.; Guo, M.; Yu, Y.; Zhai, M.; Guo, R.; Hu, J. Fabrication of coral-like Pd based Porous  $\text{MnO}_2$  nanosheet arrays on nickel foam for methanol electrooxidation. *Ind. Eng. Chem. Res.* **2018**, *57*, 10893–10904. [[CrossRef](#)]
43. Jadhav, H.S.; Roy, A.; Thorat, G.M.; Gil Seo, J. Facile and cost-effective growth of a highly efficient  $\text{MgCo}_2\text{O}_4$  electrocatalyst for methanol oxidation. *Inorg. Chem. Front.* **2018**, *5*, 1115–1120. [[CrossRef](#)]
44. Qian, L.; Luo, S.; Wu, L.; Hu, X.; Chen, W.; Wang, X. In situ growth of metal organic frameworks derived hierarchical hollow porous  $\text{Co}_3\text{O}_4/\text{NiCo}_2\text{O}_4$  nanocomposites on nickel foam as self-supported flexible electrode for methanol electrocatalytic oxidation. *Appl. Surf. Sci.* **2020**, *503*, 144306. [[CrossRef](#)]
45. Wang, X.; Li, C.; Shi, G. A high-performance platinum electrocatalyst loaded on a graphene hydrogel for high-rate methanol oxidation. *Phys. Chem. Chem. Phys.* **2014**, *16*, 10142. [[CrossRef](#)]
46. Sreekanth, T.; Ramaraghavulu, R.; Vattikuti, S.P.; Shim, J.; Yoo, K. Microwave synthesis:  $\text{ZnCo}_2\text{O}_4$  NPs as an efficient electrocatalyst in the methanol oxidation reaction. *Mater. Lett.* **2019**, *253*, 450–453. [[CrossRef](#)]
47. Shi, R.; Zhang, Y.; Wang, Z. Facile synthesis of a  $\text{ZnCo}_2\text{O}_4$  electrocatalyst with three-dimensional architecture for methanol oxidation. *J. Alloys Compd.* **2019**, *810*, 151879. [[CrossRef](#)]
48. Zhang, D.; Zhang, J.; Wang, H.; Cui, C.; Jiao, W.; Gao, J.; Liu, Y. Novel Ni foam based nickel oxalate derived porous NiO nanostructures as highly efficient electrodes for the electrooxidation of methanol/ethanol and urea. *J. Alloys Compd.* **2019**, *806*, 1419–1429. [[CrossRef](#)]
49. Sun, X.; Li, Y.; Li, M.-J. Highly dispersed palladium nanoparticles on carbon-decorated porous nickel electrode: An effective strategy to boost direct ethanol fuel cell up to 202 mW  $\text{cm}^{-2}$ . *ACS Sustain. Chem. Eng.* **2019**, *7*, 11186–11193. [[CrossRef](#)]
50. Yang, F.; Cheng, K.; Wang, G.; Cao, D. Preparation of Au nanosheets supported on Ni foam and its electrocatalytic performance towards  $\text{NaBH}_4$  oxidation. *Electrochim. Acta* **2015**, *159*, 111–115. [[CrossRef](#)]
51. Song, C.; Zhang, D.; Wang, B.; Cai, Z.; Yan, P.; Sun, Y.; Ye, K.; Cao, D.; Cheng, K.; Wang, G. Uniformly grown PtCo-Modified  $\text{Co}_3\text{O}_4$  nanosheets as a highly efficient catalyst for sodium borohydride electrooxidation. *Nano Res.* **2016**, *9*, 3322–3333. [[CrossRef](#)]

52. Ye, K.; Zhang, D.; Zhang, H.; Cheng, K.; Wang, G.; Cao, D. Platinum-Modified cobalt nanosheets supported on three-dimensional carbon sponge as a high-performance catalyst for hydrogen peroxide electroreduction. *Electrochim. Acta* **2015**, *178*, 270–279. [[CrossRef](#)]
53. Li, Y.; He, Y. Layer reduction method for fabricating Pd-Coated Ni foams as high-performance ethanol electrode for anion-exchange membrane fuel cells. *RSC Adv.* **2014**, *4*, 16879–16884. [[CrossRef](#)]
54. Verlato, E.; Cattarin, S.; Comisso, N.; Gambirasi, A.; Musiani, M.; Vázquez-Gómez, L. Preparation of Pd-Modified Ni foam electrodes and their use as anodes for the oxidation of alcohols in basic media. *Electrocatalysis* **2011**, *3*, 48–58. [[CrossRef](#)]
55. Gamil, S.; El Rouby, W.M.A.; Antuch, M.; Zedan, I.T. Nanohybrid layered double hydroxide materials as efficient catalysts for methanol electrooxidation. *RSC Adv.* **2019**, *9*, 13503–13514. [[CrossRef](#)]
56. Yuan, G.; Wang, L.; Zhang, X.; Wang, Q. Self-Supported Pt nanoflakes-doped amorphous Ni(OH)<sub>2</sub> on Ni foam composite electrode for efficient and stable methanol oxidation. *J. Colloid Interface Sci.* **2019**, *536*, 189–195. [[CrossRef](#)]
57. Du, J.; You, S.; Li, X.; Tang, B.; Jiang, B.; Yu, Y.; Cai, Z.; Ren, N.; Zou, J. In situ crystallization of active NiOOH/CoOOH hetero-structures with hydroxide ion adsorption sites on velutipes-like CoSe/NiSe nanorods as catalysts for oxygen evolution and Co-Catalysts for methanol oxidation. *ACS Appl. Mater. Interfaces* **2020**, *12*, 686–697. [[CrossRef](#)] [[PubMed](#)]
58. Niu, X.; Zhao, H.; Lan, M. Palladium deposits spontaneously grown on nickel foam for electro-catalyzing methanol oxidation: Effect of precursors. *J. Power Sources* **2016**, *306*, 361–368. [[CrossRef](#)]
59. Niu, X.; Xiong, Q.; Li, X.; Zhang, W.; He, Y.; Pan, J.; Qiu, F.; Yan, Y. Incorporating Ag into Pd/Ni Foam via cascade galvanic replacement to promote the methanol electro-oxidation reaction. *J. Electrochem. Soc.* **2017**, *164*, F651–F657. [[CrossRef](#)]
60. Guo, M.; Yu, Y.; Hu, J. Enhanced electrooxidation of methanol via ion implantation of Co nanoparticles onto 3D Ni foam templates. *J. Electrochem. Soc.* **2017**, *164*, H198–H202. [[CrossRef](#)]
61. Jadhav, H.S.; Roy, A.; Chung, W.-J.; Gil Seo, J. Free standing growth of MnCo<sub>2</sub>O<sub>4</sub> nanoflakes as an electrocatalyst for methanol electro-oxidation. *New J. Chem.* **2017**, *41*, 15058–15063. [[CrossRef](#)]
62. Jadhav, H.S.; Roy, A.; Chung, W.-J.; Gil Seo, J. Growth of urchin-like ZnCo<sub>2</sub>O<sub>4</sub> microspheres on nickel foam as a binder-free electrode for high-performance supercapacitor and methanol electro-oxidation. *Electrochim. Acta* **2017**, *246*, 941–950. [[CrossRef](#)]
63. Zhong, C.; Hu, W.B.; Cheng, Y.F. Recent advances in electrocatalysts for electro-oxidation of ammonia. *J. Mater. Chem. A* **2013**, *1*, 3216–3238. [[CrossRef](#)]
64. Wang, Y.; Zou, S.; Cai, W.-B. Recent advances on electro-oxidation of ethanol on Pt-And Pd-Based catalysts: From reaction mechanisms to catalytic materials. *Catalysts* **2015**, *5*, 1507–1534. [[CrossRef](#)]
65. Gu, L.; Qian, L.; Lei, Y.; Wang, Y.; Li, J.; Yuan, H.; Xiao, D. Microwave-Assisted synthesis of nanosphere-like NiCo<sub>2</sub>O<sub>4</sub> consisting of porous nanosheets and its application in electro-catalytic oxidation of methanol. *J. Power Sources* **2014**, *261*, 317–323. [[CrossRef](#)]
66. Wang, W.; Chu, Q.; Zhang, Y.; Zhu, W.; Wang, X.; Liu, X. Nickel foam supported mesoporous NiCo<sub>2</sub>O<sub>4</sub> arrays with excellent methanol electro-oxidation performance. *New J. Chem.* **2015**, *39*, 6491–6497. [[CrossRef](#)]
67. Tomboc, G.M.; Abebe, M.W.; Baye, A.F.; Kim, H. Utilization of the superior properties of highly mesoporous PVP modified NiCo<sub>2</sub>O<sub>4</sub> with accessible 3D nanostructure and flower-like morphology towards electrochemical methanol oxidation reaction. *J. Energy Chem.* **2019**, *29*, 136–146. [[CrossRef](#)]
68. Hassan, D.K.; El-Safty, S.A.; Khalil, K.A.; Dewidar, M.; Abu El-Maged, G. Mesoporous Carbon/Co<sub>3</sub>O<sub>4</sub> hybrid as efficient electrode for methanol electrooxidation in alkaline conditions. *Int. J. Electrochem. Sci.* **2016**, *11*, 8374–8390. [[CrossRef](#)]
69. Roy, A.; Jadhav, H.S.; Thorat, G.M.; Seo, J.G. Electrochemical growth of Co(OH)<sub>2</sub> nanoflakes on Ni foam for methanol electrooxidation. *New J. Chem.* **2017**, *41*, 9546–9553. [[CrossRef](#)]
70. Yuan, G.; Niu, X.; Chen, Z.; Wang, L.; Zhang, X.; Wang, Q. Self-Supported hierarchical shell@core Ni<sub>3</sub> S<sub>2</sub> @Ni foam composite electrocatalyst with high efficiency and long-term stability for methanol oxidation. *ChemElectroChem* **2018**, *5*, 2376–2382. [[CrossRef](#)]
71. Moura, A.S.; Fajín, J.L.C.; Mandado, M.; Cordeiro, M.N.D.S. Ruthenium-Platinum catalysts and direct methanol fuel cells (DMFC): A review of theoretical and experimental breakthroughs. *Catalysts* **2017**, *7*, 47. [[CrossRef](#)]
72. Xiao, J.; Zhang, X.; Gao, T.; Zhou, C.; Xiao, D. Electrochemical formation of multilayered NiO film/Ni foam as a high-efficient anode for methanol electrolysis. *J. Solid State Electrochem.* **2017**, *21*, 2301–2311. [[CrossRef](#)]
73. Luo, Q.; Peng, M.; Sun, X.; Asiri, A.M. Hierarchical nickel oxide nanosheet@nanowire arrays on nickel foam: An efficient 3D electrode for methanol electro-oxidation. *Catal. Sci. Technol.* **2015**, *6*, 1157–1161. [[CrossRef](#)]
74. Cheng, Y.; Zhai, M.; Hu, J. The fabrication of NiCu<sub>2</sub>S<sub>2</sub> from NiCu film on Nickel foam for methanol electrooxidation and supercapacitors. *Appl. Surf. Sci.* **2019**, *480*, 505–513. [[CrossRef](#)]
75. Hong, F.; Wang, M.; Ni, Y. NiO-CoO hybrid nanostructures: Preparation, characterization and application in methanol electrooxidation. *J. Clust. Sci.* **2018**, *29*, 663–672. [[CrossRef](#)]
76. Gao, S.; Yang, X.; Wei, M.-J.; Liang, S.; Zang, H.-Y.; Tan, H.-Q.; Wang, Y.-H.; Li, Y.-G. One-Step synthesis of Pt based electrocatalysts encapsulated by polyoxometalate for methanol oxidation. *New J. Chem.* **2018**, *42*, 198–203. [[CrossRef](#)]
77. Yu, M.; Chen, J.; Liu, J.; Li, S.; Ma, Y.; Zhang, J.; An, J. Mesoporous NiCo<sub>2</sub>O<sub>4</sub> nanoneedles grown on 3D graphene-nickel foam for supercapacitor and methanol electro-oxidation. *Electrochim. Acta* **2015**, *151*, 99–108. [[CrossRef](#)]
78. Thoufeeq, S.; Rastogi, P.K.; Sreekanth, N.; Anantharaman, M.M.R.I.; Narayanan, T.N. Nickel-Reduced graphene oxide composite foams for electrochemical oxidation processes: Towards biomolecule sensing. *MRS Commun.* **2018**, *8*, 695–702. [[CrossRef](#)]
79. Sesu, D.C.; Patil, I.M.; Lokanathan, M.; Parse, H.B.; Marbaniang, P.; Kakade, B.A. Low density three-dimensional metal foams as significant electrocatalysts toward methanol oxidation reaction. *ACS Sustain. Chem. Eng.* **2018**, *6*, 2062–2068. [[CrossRef](#)]

80. Zhu, Y.; Zhang, X.; Li, J.; Qi, G. Three-Dimensional graphene as gas diffusion layer for micro direct methanol fuel cell. *Int. J. Mod. Phys. B* **2018**, *32*, 1850145. [[CrossRef](#)]
81. Li, Y.; Lv, J.; He, Y. A monolithic carbon foam-supported Pd-Based catalyst towards ethanol electro-oxidation in alkaline media. *J. Electrochem. Soc.* **2016**, *163*, F424–F427. [[CrossRef](#)]
82. Wang, Y.-L.; Zhao, Y.-Q.; Xu, C.-L.; Zhao, D.-D.; Xu, M.-W.; Su, Z.-X.; Li, H.-L. Improved performance of Pd electrocatalyst supported on three-dimensional nickel foam for direct ethanol fuel cells. *J. Power Sources* **2010**, *195*, 6496–6499. [[CrossRef](#)]
83. Li, C.; Wen, H.; Tang, P.-P.; Wen, X.-P.; Wu, L.-S.; Dai, H.-B.; Wang, P. Effects of Ni(OH)<sub>2</sub> morphology on the catalytic performance of Pd/Ni(OH)<sub>2</sub>/Ni foam hybrid catalyst toward ethanol electrooxidation. *ACS Appl. Energy Mater.* **2018**, *1*, 6040–6046. [[CrossRef](#)]
84. Pierozynski, B.; Mikolajczyk, T. Platinum dissolution and ethanol oxidation reaction on Pt-Activated nickel foam in sodium hydroxide solution. *Pol. J. Chem. Technol.* **2017**, *19*, 41–43. [[CrossRef](#)]
85. Pierozynski, B.; Mikolajczyk, T. Enhancement of ethanol oxidation reaction on Pt (PtSn)-Activated nickel foam through in situ formation of nickel oxyhydroxide layer. *Electrocatalysis* **2017**, *8*, 252–260. [[CrossRef](#)]
86. Hatamie, A.; Rezvani, E.; Rasouli, A.S.; Simchi, A. Electrocatalytic oxidation of ethanol on flexible three-dimensional interconnected Nickel/Gold composite foams in alkaline media. *Electroanalysis* **2019**, *31*, 504–511. [[CrossRef](#)]
87. Xu, H.-T.; Qiu, H.-J.; Fang, L.; Mu, Y.; Wang, Y. A novel monolithic three-dimensional graphene-based composite with enhanced electrochemical performance. *J. Mater. Chem.* **2015**, *3*, 14887–14893. [[CrossRef](#)]
88. Liu, M.; He, S.; Chen, W. Free-Standing 3D hierarchical carbon foam-supported PtCo nanowires with “Pt Skin” as advanced electrocatalysts. *Electrochim. Acta* **2016**, *199*, 218–226. [[CrossRef](#)]
89. Zhang, Z.; Dong, Y.; Wang, L.; Wang, S. Scalable synthesis of a Pd nanoparticle loaded hierarchically porous graphene network through multiple synergistic interactions. *Chem. Commun.* **2015**, *51*, 8357–8360. [[CrossRef](#)] [[PubMed](#)]
90. Tsang, C.-H.A.; Hui, K.N.; Ren, L. Deposition of Pd/Graphene aerogel on nickel foam as a binder-free electrode for direct electro-oxidation of methanol and ethanol. *J. Mater. Chem. A* **2014**, *2*, 17986–17993. [[CrossRef](#)]
91. Tsang, C.H.A.; Leung, D. Use of Pd-Pt loaded graphene aerogel on nickel foam in direct ethanol fuel cell. *Solid State Sci.* **2018**, *75*, 21–26. [[CrossRef](#)]
92. Tsang, C.H.A.; Hui, K.N. Influence of Pd1Pt<sub>x</sub> alloy NPs on graphene aerogel/nickel foam as binder-free anodic electrode for electrocatalytic ethanol oxidation reaction. *J. Power Sources* **2019**, *413*, 98–106. [[CrossRef](#)]
93. Doğan, H.Ö. Ethanol electro-oxidation in alkaline media on Pd/Electrodeposited reduced graphene oxide nanocomposite modified nickel foam electrode. *Solid State Sci.* **2019**, *98*, 106029. [[CrossRef](#)]
94. Ma, J.; Gao, X.; Li, J.; Li, H. Promoting effect of tin on binder-free CoSn<sub>x</sub>-B/Ni-foam catalysts for fuel conversion efficiency in direct borohydride fuel cell. *Fuel Cells* **2019**, *19*, 609–615. [[CrossRef](#)]
95. Guo, M.; Cheng, Y.; Yu, Y.; Hu, J. Ni-Co nanoparticles immobilized on a 3D Ni foam template as a highly efficient catalyst for borohydride electrooxidation in alkaline medium. *Appl. Surf. Sci.* **2017**, *416*, 439–445. [[CrossRef](#)]
96. Santos, D.M.F.; Eugénio, S.; Cardoso, D.S.P.; Šljukić, B.; Montemor, M.F. Three-Dimensional nanostructured Ni–Cu foams for borohydride oxidation. *Russ. J. Phys. Chem. A* **2015**, *89*, 2449–2454. [[CrossRef](#)]
97. Gouveia, W.; Bello, M.; Balčiūnaitė, A.; Eugénio, S.; Santos, D.M.F. 3d metallic foams as catalysts for hydrolysis and electrooxidation of sodium borohydride. *ECS Trans.* **2018**, *86*, 603–612. [[CrossRef](#)]
98. Li, B.; Song, C.; Huang, X.; Ye, K.; Cheng, K.; Zhu, K.; Yan, J.; Cao, D.; Wang, G. A novel anode for direct borohydride-hydrogen peroxide fuel cell: Au nanoparticles decorated 3d self-supported reduced graphene oxide foam. *ACS Sustain. Chem. Eng.* **2019**, *7*, 11129–11137. [[CrossRef](#)]
99. Li, B.; Song, C.; Zhang, D.; Ye, K.; Cheng, K.; Zhu, K.; Yan, J.; Cao, D.; Wang, G. Novel self-supported reduced graphene oxide foam-based CoAu electrode: An original anode catalyst for electrooxidation of borohydride in borohydride fuel cell. *Carbon* **2019**, *152*, 77–88. [[CrossRef](#)]
100. Li, B.; Yan, Q.; Song, C.; Yan, P.; Ye, K.; Cheng, K.; Zhu, K.; Yan, J.; Cao, D.; Wang, G. Reduced graphene oxide foam supported CoNi nanosheets as an efficient anode catalyst for direct borohydride hydrogen peroxide fuel cell. *Appl. Surf. Sci.* **2019**, *491*, 659–669. [[CrossRef](#)]
101. Guo, F.; Cao, D.; Du, M.; Ye, K.; Wang, G.; Zhang, W.; Gao, Y.; Cheng, K. Enhancement of direct urea-hydrogen peroxide fuel cell performance by three-dimensional porous nickel-cobalt anode. *J. Power Sources* **2016**, *307*, 697–704. [[CrossRef](#)]
102. Ye, K.; Zhang, H.; Zhao, L.; Huang, X.; Cheng, K.; Wang, G.; Cao, D. Facile preparation of three-dimensional Ni(OH)<sub>2</sub>/Ni foam anode with low cost and its application in a direct urea fuel cell. *New J. Chem.* **2016**, *40*, 8673–8680. [[CrossRef](#)]
103. Li, J.; Yao, C.; Kong, X.; Li, Z.; Jiang, M.; Zhang, F.; Lei, X. Boosting hydrogen production by electrooxidation of urea over 3D hierarchical Ni<sub>4</sub>N/Cu<sub>3</sub>N nanotube arrays. *ACS Sustain. Chem. Eng.* **2019**, *7*, 13278–13285. [[CrossRef](#)]
104. Sha, L.; Ye, K.; Wang, G.; Shao, J.; Zhu, K.; Cheng, K.; Yan, J.; Wang, G.; Cao, D. Rational design of NiCo<sub>2</sub>S<sub>4</sub> nanowire arrays on nickel foam as highly efficient and durable electrocatalysts toward urea electrooxidation. *Chem. Eng. J.* **2019**, *359*, 1652–1658. [[CrossRef](#)]
105. Tang, C.; Zhao, Z.L.; Chen, J.; Li, B.; Chen, L.; Li, C.M. Se-Ni(OH)<sub>2</sub>-shelled vertically oriented NiSe nanowires as a superior electrocatalyst toward urea oxidation reaction of fuel cells. *Electrochim. Acta* **2017**, *248*, 243–249. [[CrossRef](#)]
106. Qian, S.; Rao, Z.; Liu, Y.; Yan, J.; Fan, B.; Gui, Y.; Guo, F. Nickel-Rhodium bimetallic dispersions supported on nickel foam as the efficient catalyst for urea electrooxidation in alkaline medium. *Electrochim. Acta* **2020**, *330*, 135211. [[CrossRef](#)]

107. Yan, X.; Zhang, W.-D.; Hu, Q.-T.; Liu, J.; Li, T.; Liu, Y.; Gu, Z.-G. Defects-Rich nickel nanoparticles grown on nickel foam as integrated electrodes for electrocatalytic oxidation of urea. *Int. J. Hydrog. Energy* **2019**, *44*, 27664–27670. [[CrossRef](#)]
108. Zhan, S.; Zhou, Z.; Liu, M.; Jiao, Y.; Wang, H. 3D NiO nanowalls grown on Ni foam for highly efficient electro-oxidation of urea. *Catal. Today* **2019**, *327*, 398–404. [[CrossRef](#)]
109. Sha, L.; Ye, K.; Wang, G.; Shao, J.; Zhu, K.; Cheng, K.; Yan, J.; Wang, G.; Cao, D. Hierarchical NiCo<sub>2</sub>O<sub>4</sub> nanowire array supported on Ni foam for efficient urea electrooxidation in alkaline medium. *J. Power Sources* **2019**, *412*, 265–271. [[CrossRef](#)]
110. Liu, X.; Hao, M.; Feng, M.; Zhang, L.; Zhao, Y.; Du, X.; Wang, G. A one-compartment direct glucose alkaline fuel cell with methyl viologen as electron mediator. *Appl. Energy* **2013**, *106*, 176–183. [[CrossRef](#)]
111. Yang, Y.-L.; Liu, X.-H.; Hao, M.-Q.; Zhang, P.-P. Performance of a low-cost direct glucose fuel cell with an anion-exchange membrane. *Int. J. Hydrog. Energy* **2015**, *40*, 10979–10984. [[CrossRef](#)]
112. Chen, J.; Zhao, C.X.; Zhi, M.M.; Wang, K.; Deng, L.; Xu, G. Alkaline direct oxidation glucose fuel cell system using silver/nickel foams as electrodes. *Electrochim. Acta* **2012**, *66*, 133–138. [[CrossRef](#)]
113. Li, Z.; Liu, X.; Liu, P.; Zhang, P. The performance of electron-mediator modified activated carbon as anode for direct glucose alkaline fuel cell. *Catalysts* **2016**, *6*, 95. [[CrossRef](#)]
114. Chen, J.; Zheng, H.; Kang, J.; Yang, F.; Cao, Y.; Xiang, M. An alkaline direct oxidation glucose fuel cell using three-dimensional structural Au/Ni-foam as catalytic electrodes. *RSC Adv.* **2017**, *7*, 3035–3042. [[CrossRef](#)]
115. Tsang, C.H.A.; Leung, D. Pd-Pt loaded graphene aerogel on nickel foam composite as binder-free anode for a direct glucose fuel cell unit. *Solid State Sci.* **2017**, *71*, 123–129. [[CrossRef](#)]
116. Zhao, Y.; Liu, X.; Wang, X.; Zhang, P.; Shi, J. Peony petal-like 3D graphene-nickel oxide nanocomposite decorated nickel foam as high-performance electrocatalyst for direct glucose alkaline fuel cell. *Int. J. Hydrog. Energy* **2017**, *42*, 29863–29873. [[CrossRef](#)]
117. Wu, W.; Miao, F.; Tao, B.; Zang, Y.; Zhu, L.; Shi, C.; Chu, P.K. Hybrid ZnO-Graphene electrode with palladium nanoparticles on Ni foam and application to self-powered nonenzymatic glucose sensing. *RSC Adv.* **2019**, *9*, 12134–12145. [[CrossRef](#)]
118. Rice, C.A.; Urchaga, P.; Pistono, A.O.; McFerrin, B.W.; McComb, B.T.; Hu, J. Platinum dissolution in fuel cell electrodes: Enhanced degradation from surface area assessment in automotive accelerated stress tests. *J. Electrochem. Soc.* **2015**, *162*, 1175–1180. [[CrossRef](#)]
119. El-Nagar, G.A.; Derr, I.; Kottakkat, T.; Roth, C. Auspicious metal-doped-Cu<sub>2</sub>O/Cu dendrite (M = Ni, Co, Fe) catalysts for direct alkaline fuel cells: Effect of dopants. *ECS Trans.* **2017**, *80*, 1013–1022. [[CrossRef](#)]
120. Song, C.; Cao, L.; Li, B.; Huang, X.; Ye, K.; Zhu, K.; Cao, D.; Cheng, K.; Wang, G. Highly efficient palladium nanoparticles decorated reduced graphene oxide sheets supported on nickel foam for hydrogen peroxide electroreduction. *Appl. Surf. Sci.* **2017**, *426*, 1046–1054. [[CrossRef](#)]
121. Yang, F.; Cao, B.; Tao, Y.; Cao, D.; Zhang, Y. Nicotinamide-Assisted fabrication of high-stability gold-palladium nanoparticles on carbon fiber cloth for hydrogen peroxide electroreduction. *Electrochim. Acta* **2016**, *210*, 199–205. [[CrossRef](#)]
122. Xiao, X.; Yang, F.; Cheng, K.; Wang, X.; Zhang, H.; Ye, K.; Wang, G.; Cao, D. Enhanced performance of direct peroxide/peroxide fuel cell by using ultrafine nickel ferric ferrocyanide nanoparticles as the cathode catalyst. *Int. J. Hydrog. Energy* **2017**, *42*, 22856–22865. [[CrossRef](#)]
123. Yang, Y.; Dong, R.; Zhu, Y.; Li, H.; Zhang, H.; Fan, X.; Chang, H. High-Performance direct hydrogen peroxide fuel cells (DHPFCs) with silver nanowire-graphene hybrid aerogel as highly-conductive mesoporous electrodes. *Chem. Eng. J.* **2020**, *381*, 122749. [[CrossRef](#)]
124. Sun, L.; He, W.; Li, S.; Shi, L.; Zhang, Y.; Liu, J. The high performance mushroom-like Pd@SnO<sub>2</sub>/Ni foam electrode for H<sub>2</sub>O<sub>2</sub> reduction in alkaline media. *J. Power Sources* **2018**, *395*, 386–394. [[CrossRef](#)]
125. Yang, F.; Cheng, K.; Xue, X.; Yin, J.; Wang, G.; Cao, D. Three-Dimensional porous Ni film electrode deposited on Ni foam: High performance and low-cost catalytic electrode for H<sub>2</sub>O<sub>2</sub> electrooxidation in KOH solution. *Electrochim. Acta* **2013**, *107*, 194–199. [[CrossRef](#)]
126. Xiao, X.; Yang, F.; Cheng, K.; Wang, X.; Yin, J.; Ye, K.; Wang, G.; Cao, D. NiCo<sub>2</sub>O<sub>4</sub> nanostructures with various morphologies as the high-performance electrocatalysts for H<sub>2</sub>O<sub>2</sub> electroreduction and electrooxidation. *J. Electroanal. Chem.* **2014**, *729*, 103–108. [[CrossRef](#)]
127. Cheng, K.; Cao, D.; Yang, F.; Xu, Y.; Sun, G.; Ye, K.; Yin, J.; Wang, G. Facile synthesis of morphology-controlled Co<sub>3</sub>O<sub>4</sub> nanostructures through solvothermal method with enhanced catalytic activity for H<sub>2</sub>O<sub>2</sub> electroreduction. *J. Power Sources* **2014**, *253*, 214–223. [[CrossRef](#)]
128. Shih, Y.-J.; Huang, Y.-H.; Huang, C. In-Situ electrochemical formation of nickel oxyhydroxide (NiOOH) on metallic nickel foam electrode for the direct oxidation of ammonia in aqueous solution. *Electrochim. Acta* **2018**, *281*, 410–419. [[CrossRef](#)]
129. Wen, H.; Gan, L.-Y.; Dai, H.-B.; Wen, X.-P.; Wu, L.-S.; Wu, H.; Wang, P. In situ grown Ni phosphide nanowire array on Ni foam as a high-performance catalyst for hydrazine electrooxidation. *Appl. Catal. B Environ.* **2019**, *241*, 292–298. [[CrossRef](#)]
130. Feng, Z.; Li, D.; Wang, L.; Sun, Q.; Lu, P.; Xing, P.; An, M. In situ grown nanosheet NiZn alloy on Ni foam for high performance hydrazine electrooxidation. *Electrochim. Acta* **2019**, *304*, 275–281. [[CrossRef](#)]
131. Zhao, M.; Li, H.; Li, W.; Li, J.; Yi, L.; Hu, W.; Li, C.M. Ru-Doping enhanced Electrocatalysis of metal-organic framework nanosheets toward overall water splitting. *Chem. A Eur. J.* **2020**, *26*, 17091–17096. [[CrossRef](#)]

132. Cheng, X.; Yuan, J.; Cao, J.; Lei, C.; Yang, B.; Li, Z.; Zhang, X.; Yuan, C.; Lei, L.; Hou, Y. Strongly coupling of amorphous/crystalline reduced FeOOH/ $\alpha$ -Ni(OH)<sub>2</sub> heterostructure for extremely efficient water oxidation at ultra-high current density. *J. Colloid Interface Sci.* **2020**, *579*, 340–346. [[CrossRef](#)] [[PubMed](#)]
133. Park, Y.S.; Lee, J.H.; Jang, M.J.; Jeong, J.; Park, S.M.; Choi, W.-S.; Kim, Y.; Yang, J.; Choi, S.M. Co<sub>3</sub>S<sub>4</sub> nanosheets on Ni foam via electrodeposition with sulfurization as highly active electrocatalysts for anion exchange membrane electrolyzer. *Int. J. Hydrog. Energy* **2020**, *45*, 36–45. [[CrossRef](#)]
134. Wang, W.; Yang, Z.; Jiao, F.; Gong, Y. (P, W)-Codoped MoO<sub>2</sub> nanoflowers on nickel foam as an efficient bifunctional electro-catalyst for overall water splitting. *Appl. Surf. Sci.* **2020**, *529*, 146987. [[CrossRef](#)]